CHALMERS

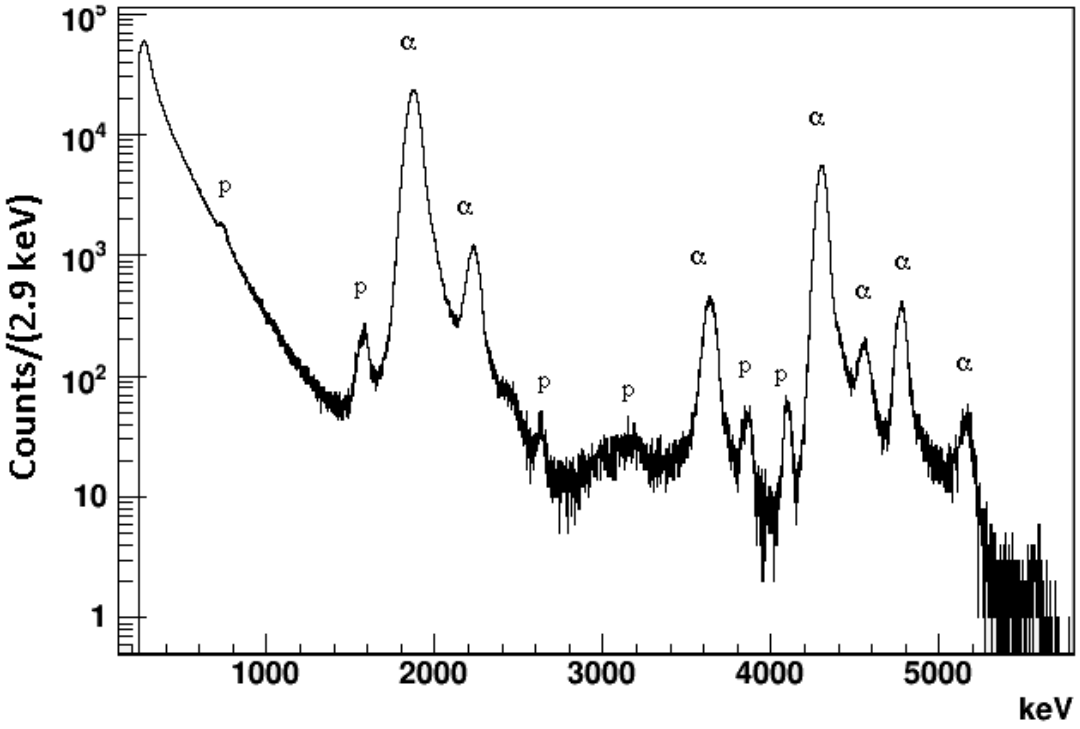

Analysis of experimental data on β-delayed proton and α-particle emission

Master Thesis in Fundamental Physics

MALIN KLINTEFJORD

Department of Fundamental Physics
Subatomic Physics
Chalmers University of Technology
Gothenburg, Sweden 2012

Analysis of experimental data on β-delayed proton and α-particle emission
MALIN KLINTEFJORD

Department of Fundamental Physics
Chalmers University of Technology

SE-412 96 Göteborg
Sweden
Telephone + 46(0)31-772 1000

Cover:
Figure 10. The energy spectrum off all detected events in the first silicon detector from the decay of ^{20}Mg. In the spectrum strong α-peaks from the decay of ^{20}Na are seen as well as a continuous distribution due to β-decay. The two strongest proton peaks can be seen around 806 keV and 1670 keV.

Chalmers Reproservice
Göteborg, Sweden 2012

Acknowledgments

A great thanks to my inspiring and wise supervisor Thomas Nilsson. Thanks also to Boris Carlsson, Hans Fynbo, Andreas Heinz, Håkan Johansson, Björn Jonson, Morten Lund, Karsten Riisager, Göran Nyman, Olof Tengblad and Ronja Thies for all the advice and help.

Abstract

The spin and parity of the resonance level 2645 keV in ^{20}Na have been studied and discussed for decades among physicists, due to the astrophysical importance of the ^{19}Ne(p,γ)^{20}Na reaction. The level is situated 450 keV above the threshold for (^{19}Ne+p).

In this thesis data from an experiment investigating ^{20}Mg β-delayed proton emission, done at CERN-ISOLDE, has been calibrated and analyzed in order to obtain pure proton spectra in search for the resonance level. Simulations of energy deposition in the detectors have also been performed for the setup used and for potential future setups.

It was found that the setup used was not sufficiently sensitive to put new limits on the population of the 2645 keV state. Therefore different detectors are discussed, which could allow to lower the amount of detected β-background and recoils of ^{16}O, from the decay of ^{20}Na.

New findings were α-particles from β-delayed α-emission from ^{21}Mg, identified in the used $\Delta E - E$ telescope.

Keywords: ^{20}Mg, β-delayed, proton emission, detectors, calibration, spectra, coincidence.

Contents

1 Introduction

The Subatomic Physics group at Chalmers University of Technology is active in studies of exotic nuclei in the vicinity of the neutron and proton drip lines. Present experiments are done at the ISOLDE facility at CERN and the heavy-ion accelerator SIS at GSI. The main collaborators, concerning the CERN experiments are from Aarhus University in Denmark and the Spanish Insitituto de Estructura de la Materia at CSIC in Madrid.

Recent developments of better detectors have increased the possibility of particle identification at low energies. Those might be used to distinguish between protons, other decay products and background in order to find, or put limits to, branching ratios in radioactive nuclei. Due to the astrophysical importance of the spin and parity of the resonance level at 2645 keV in ^{20}Na, an attempt to study β-delayed proton emission is of interest for the research group.

1.1 Purpose

The purpose of this Master thesis is to analyze data taken during the IS507 experiment at CERN-ISOLDE in November 2011. The main focus is on calibration of the used detectors and on extracting pure proton spectra at low energies in search for the 450 keV β-delayed proton-line from ^{20}Mg.

1.2 Outline

The thesis starts with a theoretical background in Section 2, dealing with why the decay of ^{20}Mg has been in focus for many years and how it has been studied in the past. Section 3 gives an introduction to charged-particle detection and detectors related to the analyzed experiment. The experiment and setup are explained in Section 4.

Section 5 is dedicated to the calibration of the detectors and in Section 6 the creation of the energy spectra with different cuts is treated. In Section 7 Monte Carlo simulations of detected energy from the decay, done in GEANT3, are shown.

Finally the results of this work is presented in Section 8 and further discussed in Section 9. The main conclusions are summarized in Section 10.

2 Theoretical Background

2.1 ^{20}Mg and its astrophysical importance

The unstable nucleus ^{20}Mg is located at the proton drip line. In the Universe, ^{20}Mg is found in dense stellar environments with temperatures over 10^8 K. It decays via β^+-decay to ^{20}Na with a half-life of 90.8 ms [1]. Subsequently, ^{20}Na decays via β^+-decay to ^{20}Ne or via β^+-delayed α-emission to ^{16}O. The half-life of ^{20}Na is about 447.9 ms [1].

The location of ^{20}Mg in a chart of nuclides is shown in Figure 1, where isotopes are color coded according to their decay mode. The isotope ^{20}Mg can also decay via β^+-delayed proton emission to (^{19}Ne + p). This reaction is part of a breakout from the Hot Carbon-Nitrogen–Oxygen-cycle (HCNO) and seeds the creation of heavier elements in the rapid proton capture (rp)-process [2].

The HCNO-cycle occurs for example near X-ray-emitting binary stars, called X-ray bursts. Hydrogen is converted into helium through one of the catalytic processes given in reactions (1-3):

$$^{12}\mathrm{C}(p,\gamma)^{13}\mathrm{N}(p,\gamma)^{14}\mathrm{O}(e^+,\nu)^{14}\mathrm{N}(p,\gamma)^{15}\mathrm{O}(e^+,\nu)^{15}\mathrm{N}(p,\alpha)^{12}\mathrm{C}, \quad (1)$$

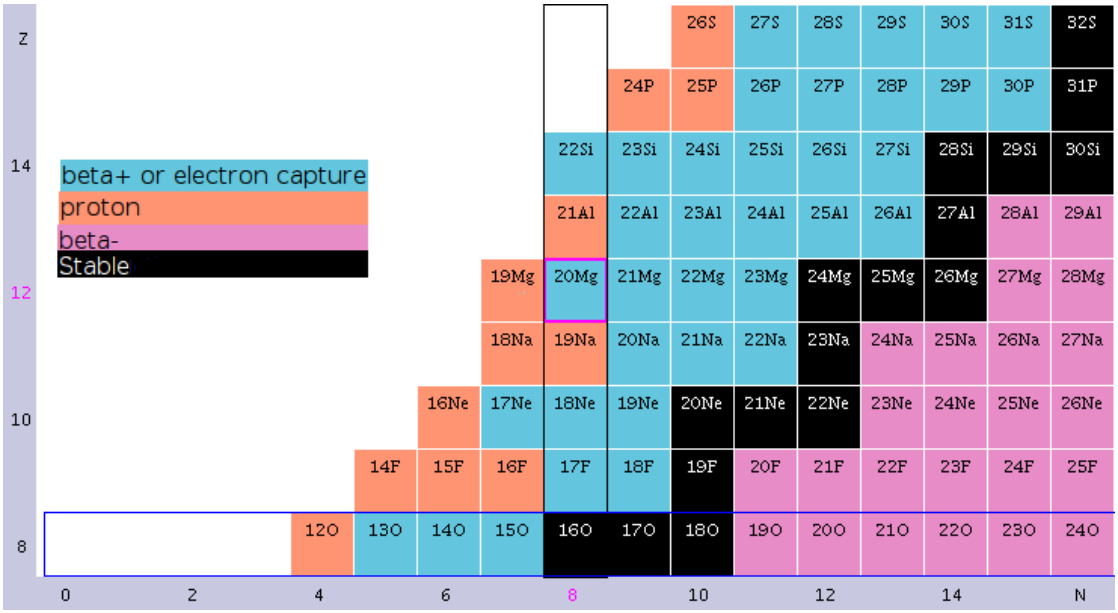

Figure 1: The location of ^{20}Mg in the chart of nuclides, where isotopes are color coded according to their decay mode.

$$^{15}\mathrm{O}(e^+,\nu)^{15}\mathrm{N}(p,\gamma)^{16}\mathrm{O}(p,\gamma)^{17}\mathrm{F}(e^+,\nu)^{17}\mathrm{O}(p,\gamma)^{18}\mathrm{F}(p,\alpha)^{15}\mathrm{O}, \tag{2}$$

$$^{15}\mathrm{O}(e^+,\nu)^{15}\mathrm{N}(p,\gamma)^{16}\mathrm{O}(p,\gamma)^{17}\mathrm{F}(p,\gamma)^{18}\mathrm{Ne}(e^+,\nu)^{18}\mathrm{F}(p,\alpha)^{15}\mathrm{O}. \tag{3}$$

One important breakout reaction is ^{15}O(α,γ)^{19}Ne. If ^{19}Ne absorbs a proton and forms ^{20}Na, before β^+-decaying to ^{19}F it leaves the HCNO-cycle [3]. The limit of how many protons that can be absorbed in the rp-process depends on the environment temperature, but a theoretical limit has been set for proton number $Z \leq 54$ [4].

The lowest excited state in ^{20}Na, with excitation energy above the threshold for proton emission to (^{19}Ne + p) is located at an energy of 2645 keV, exceeding the threshold by 450 keV[1]. The spin and parity of this state has earlier been determined to be either $J^\pi = 1^+$ or $J^\pi = 3^+$ [2]. The level scheme for the decay of ^{20}Mg, as given by [1] is shown in Figure 2.

The strength of the resonances of ^{19}Ne(p,γ)^{20}Na is defined as

$$\omega\gamma = \frac{2J+1}{(2J_1+1)(2J_2+1)} \cdot \frac{\Gamma_\gamma \Gamma_p}{(\Gamma_\gamma + \Gamma_p)} \tag{4}$$

where J_1 and J_2 are the spin of the projectile and the target nuclei. J is the spin of the resonant state and Γ_γ and Γ_p are the widths of the γ- and proton decay channels of the same level [2]. As can be seen from Equation (4), the spin of the resonance state is important for the breakout rate.

[1] At the very end of the writing of this thesis, new research results were published by J.P Wallace et al. in β-delayed proton decay study of ^{20}Mg and its implications for the ^{19}Ne(p,γ)^{20}Na breakout reaction in X-ray burst. (2012) *Physics Letters*, B712, 59-62. Those results have not been taken into account before the publication of this thesis.

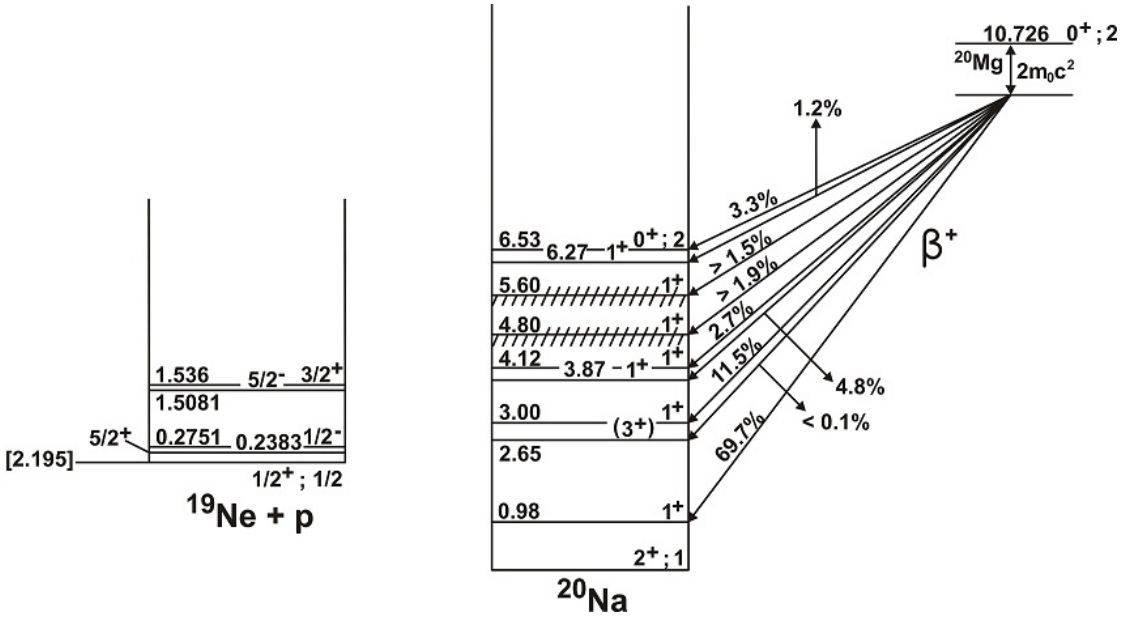

Figure 2: The level scheme for ^{20}Mg decay, from [1].

2.2 Proton energy

Since β-decay is a three-body problem, the energy of the electron or positron will form a continuous spectrum. The delayed particle emission, however, is a two-body decay into particle and daughter nucleus. The particle and the daughter will therefore be emitted with distinct energies. Their total kinetic energy is equal to the difference between the energy level in the mother- and daughter nucleus. The energy of a proton emitted from ^{20}Na can be calculated from conservation of energy and momentum [5], and is given by Equation (5),

$$E_p = (E_{\text{ex}} - S_p)(\frac{M_{\text{Ne}}}{M_p + M_{\text{Ne}}}) \tag{5}$$

where E_{ex} is the excitation energy in ^{20}Na, S_p is the proton separation energy of ^{20}Na and M_p and M_{Ne} are the masses of a proton and ^{19}Ne respectively. The most intensive delayed proton peak has previously been measured to be at $E_{\text{ex}} - S_p = 806$ keV while the second most intensive peak is located at $E_{\text{ex}} - S_p = 1670$ keV [2]. This corresponds to $E_p = 765$ keV and $E_p = 1586$ keV. Protons with $E_{\text{ex}} - S_p = 450$ keV are further expected to have $E_p = 427$ keV.

The fact that levels at high excitation energy often lie very close to each other leads to a spectrum that appears more like a continuum, similar to a β-spectrum. Therefore, instead of talking about distinct energies, a β-decay strength function with the average β-decay intensity that leads to a region of excited states is often used.

2.3 Fermi and Gamow-Teller decay

The β-decay strength is approximately proportional to the density of states, while one state is dominant because of its large Fermi matrix element. This state is called the Isobaric Analog State (IAS) [5].

The allowed approximation for β-decay assumes that the electron or positron and the antineutrino or neutrino are emitted without carrying any angular momentum so only the intrinsic spin $s = \frac{1}{2}$ of the leptons contributes. The decay rate depends on the interaction, V, between the wave function, ψ, for the initial and the final state.

$$V_{fi} = \int \psi_f^* V \psi_i dv \tag{6}$$

The integral in Equation (6) is called the matrix element for the decay. In the allowed decay, when the wave functions of the electron (positron) and antineutrino (neutrino) are approximated as plane waves, the rate can also be expressed as a function of the nuclear matrix element, given by Equation (7).

$$V_{fi} = g \int [\psi_f^* \phi_e^* \phi_v] O_x \psi_i dv \tag{7}$$

In this case ψ represents the nuclear wave function while ϕ_e and ϕ_v are the wave functions for the electron (positron) and antineutrino (neutrino), respectively. Here O_x, is the operator of the weak interaction and g is the strength of the decay. Equation (8)

$$f(Z, E_0) = \frac{1}{(m_e c)^3 (m_e c^2)^2} \int_0^{p_{max}} F(Z,p) p^2 (E_0 - E_e)^2 dp \tag{8}$$

is called the Fermi integral and gives a constant part of the decay rate for a certain β-decay. Here Z is the number of protons in the nucleus, E_0 is the maximum total electron energy, E_e is the electron energy, m_e is the mass of the electron, c is the speed of light in vacuum and p is the electron momentum. F is the Fermi function taking into account the nuclear Coulomb field. The logarithm of f multiplied with the half-life $t_{1/2}$ is often used to compare the probability of decay to different states.

For a Fermi decay the spin of the electron (positron) and antineutrino (neutrino) are antiparallel which gives a total spin $S = 0$. To fulfill angular momentum conservation in the decay process, the change in total spin, J, between mother and daughter has to be zero. If the neutrino (antineutrino) and the electron (positron) have parallel spins, then $S = 1$ and angular momentum conservation allows $\Delta J = 0$ or $\Delta J = 1$, (except for the case with both mother and daughter having $J = 0$). This is known as Gamow-Teller decay. The case with $\Delta J = 0$ can correspond to both Fermi and Gamow-Teller decays and there may be a mixed transition.

If the spin and parity of the resonance level is 1^+, the β-decay from the ground state 0^+ in ^{20}Mg corresponds to an allowed Gamow-Teller decay and therefore the level at 2645 keV in ^{20}Na is strongly populated. In previous studies, an upper limit of 0.1% for the branching ratio to this state has been measured [2]. This corresponds to a log(ft) value greater than 6.2. Populating a 1^+ level should correspond to a log(ft) value of about 4, and a $J^\pi = 3^+$ would give log(ft) of about 12. In order to fully exclude a 1^+-state a lower limit of log(ft) between 7 and 8 is necessary [2]. Cases with allowed decays and log(ft) greater than 6 have previously been found in, for example, ^{17}Ne and are explained by level mixing in the shell model [6].

2.4 Shell model calculations

The shell model is based on the experimental observation that some proton numbers in a nucleus give very high proton separation energy. The same phenomenon is also observed for the neutron numbers and neutron separation energy. Those numbers (2, 8, 20, 28, 50, 82 and 126) are called magic numbers and are said to form 'shells' in the nucleus. It seems that nucleons in nuclei can

be treated very similar to electrons in the atomic shell model, if neutrons and protons are treated independently. The angular momentum l gives orbits in the shell model named (s, p, d, f, g, h) for $l = (0, 1, 2, 3, 4, 5)$. The strong nuclear interaction and the spin-orbit interaction, coupling the angular momentum to the spin of the nucleons, s, gives a potential, which can explain the magic numbers theoretically [5].

The starting point for a shell model for nuclei is the assumption of a configuration of nucleons up to a magic number contained within a closed shell. For ^{20}Na with $Z = 11$ protons and $N = 9$ neutrons, that means two protons and two neutrons in the first s-orbital, four protons and four neutrons in the first p-orbital, 3 valence protons and 1 valence neutron in the second s- or first d-orbital. Assuming valence nucleons in 2s1d is called sd-model space and this space is applicable for nuclei with the number of nucleons, A, from 16 up to 40 [7].

The shell model calculations consist of two parts. First the calculation of the mean field from the nucleon-nucleon interaction, which is called single-particle matrix element, and then the calculation of the two-body matrix element. The single matrix element is often taken from experimental measurements, but for nuclei near the drip line those are not known and have to be calculated using, for example the Hartree Fock approximation. A so called G-matrix, representing the short range interaction between two nucleons, is often used to obtain the two-body matrix elements [7].

The first sd-shell model has been proposed in 1960 by Kuo and Brown and in 1984 the first set of unique two-body matrix elements that represent the whole sd-space was calculated by Wildenthal [7].

Within the G-matrix method it is possible to take into account intruder states, which occur due to mixing with single-particle levels outside the sd-space. This can be done by renormalization of the G-matrix and is an important step for nuclei near magic numbers. One difficulty with shell-model calculations is to also include three-body forces, which cannot be neglected for certain nuclei [7].

2.5 Isospin mirror symmetry

The first reaction studies of ^{19}Ne(p,γ)^{20}Na determined the 2645 keV state to have $J^\pi = 1^+$ [2]. $J^\pi = 3^+$ was suggested in 1993 by Brown et al. [8] after studying Coulomb shift systematics. The conclusion from this study is based on the isospin[2] mirror symmetry with the 3^+ state in ^{20}F that has a low decay probability from ^{20}O. Isospin mirror symmetry originates from the fact that the nuclear force is almost independent of charge. The wave functions for initial and final states in Equation (6) are therefore almost the same for a β^+-decay of a nucleus with Z protons and N neutrons, and the corresponding β^--decay of its mirror nucleus, where the proton and neutron numbers are interchanged. For ^{20}Mg decaying into ^{20}Na the mirror decay is ^{20}O decaying into ^{20}F. Deviations from the symmetry appear if one of the decays is to a bound level and the other to an unbound level [5].

The symmetry has been proven experimentally for states below the resonance state, for example by measuring γ-decay in coincidence with ^{20}F and ^{20}Na [9]. In that experiment no γ-rays from states above the proton threshold in ^{20}Na were observed but ^{20}O showed a multitude of γ-peaks around the higher lying states. A 1^+ state at 2645 keV in ^{20}Na is expected to have a 93% proton decay branch while a 3^+ state is expected to have a 90% proton decay branch. For both cases that means too few γ-decays for a reliable result.

[2]Isospin reflects the charge independence of the nucleon-nucleon interaction. The protons and neutrons are in this regard seen as the same particle with the same isospin $T = \frac{1}{2}$, but different isospin projections, $T_z = +\frac{1}{2}$ for protons and $T_z = -\frac{1}{2}$ for neutrons.

The fact that the 2645 keV level is situated close to the threshold for (^{19}Ne + p) might explain why this state can be stronger populated than its isospin analogue in ^{20}F and has not necessarily $J^{\pi} = 3^{+}$ [2].

The deviation from isospin symmetry for two mirror decays, defined in Equation (9), has been extracted by Piechaczek et al. [2] to be 0.230, to the bound states in ^{20}F and ^{20}Na.

$$\frac{ft^{+}}{ft^{-}} - 1 \tag{9}$$

For the decay to an unbound state in ^{20}Na (806 keV), the deviation was in the same experiment found to be 1.69.

Theoretically, the isospin symmetry breaking can be calculated within different shell models. Starting with an isospin symmetric Hamiltonian, H_0, the isospin symmetry breaking part, V_{ISB}, can be added and calculated using perturbation theory. The strength of V_{ISB} can then be fitted to the Isobaric Mass Multiple Equation (IMME) [10], given in Equation (10),

$$E(T, T_z) = a(T) + b(T)T_z + c(T)T_z^2 \tag{10}$$

where T and T_z are the isospin and isospin projection, respectively, while a, b and c are constants.

2.6 Gamow-Teller quenching

The decay of ^{20}Mg can also be used to study the so-called quenching of the Gamow-Teller strength. The Gamow-Teller strength is defined in Equation (11) [11].

$$B(GT_{\pm}) = \frac{\mid \langle f \mid \Sigma_{k=1}^{A} \sigma_{\mu k} \tau_{\pm} k \mid i \rangle \mid^2}{2J_i + 1} \tag{11}$$

Here, the $\sigma_{\mu k}$ are the components of the Pauli spin matrices, τ is the isospin-ladder operator and k is the sum over all nucleons in the nucleus. The $\pm$ sign indicates β^{+}- respective β^{-}-decay. This holds for the non-relativistic case and under the assumption that the nucleons are structureless and point-like.

The relation between the strength and the $ft_{\pm}$ value is given by Equation (12) [7],

$$ft_{\pm} = \frac{C}{(\frac{g_A}{g_V})^2 (B(GT_{\pm})) + B(F_{\pm})} \tag{12}$$

where g_A and g_V are the axial and vector component of the strength and C is a constant.

The strength can be calculated in different shell models and the obtained value will depend on the chosen model. For the Fermi case this coincide very well with measured values. Sometimes a small correction factor, d, is added to compensate for charge dependent interactions which gives $B^{*}(F) = (1 - d)B(F)$ [7].

In general, the measured Gamow-Teller strength for a heavy nucleus seems to be lower than the theoretical value. The ratio of the experimental and theoretical values of the strength is known as the quenching factor. By comparing measured values with theoretical values calculated in sd-space, a quenching factor of about 0.59 has been found [7]. It has been suggested that the missing Gamow-Teller strength should be located in a continuum of excitation energy beyond the Gamow-Teller resonance. That is the outcome of a calculation taking the 1p1h mixing state with 2p2h into account [11]. The 1p1h (one particle-one hole) state approximation assumes that the excitation energy is generated from a one-body operator. Taking into account also a two-body

interaction 2p2h (two particles-two holes), the new Hamiltonian will consist of two parts, the mean field from the 1p1h model and one antisymmetric part [12].

One of the reasons why ^{20}Mg is a candidate for this kind of studies is that 79% of the Gamow-Teller strength are predicted from shell model calculation to be located within the window for electron capture, Q_{EC} [2].

By measuring the branching ratio, b_i, for an observed proton-line from ^{20}Mg, the partial half-life, t_i, can be obtained from Equation (13) [5],

$$t_i = \frac{t_{1/2}}{b_i} \tag{13}$$

where $t_{1/2}$ is the total half-life. With theoretical values of f and know constants, C and $\frac{g_A}{g_V}$, $B(GT_{\pm})$ can be obtained from Equation (12).

3 Particle detection

3.1 Charged particle interaction with matter

Charged particles like α's, protons or β's will lose energy when they pass through and interact with a material. The dominant part of the energy loss for a heavy charged particle is through collision with atomic electrons in the material, called Coulomb scattering. The magnitude of the energy loss can be described by the Bethe-Bloch formula [5], given in Equation (14),

$$\frac{dE}{dx} = (\frac{e^2}{4\pi\epsilon_0})^2 \frac{4\pi z^2 N_0 Z\rho}{mc^2\beta^2 A}[\ln(\frac{2mc^2\beta^2}{I}) - \ln(1-\beta^2) - \beta^2] \tag{14}$$

with the velocity of the particle $v = \beta c$, c is the speed of light in vacuum, ze is the electric charge of the particle. Z is the atomic number of the target, A is the atomic weight and ρ is the density of the stopping target. N_0 is Avogadros number, m is the electron mass and I is the mean excitation energy of the atomic electrons.

From the Bethe-Bloch formula, it can be seen that the energy loss depends on the square of the charge of the particle, and also its velocity.

How deep into a material a charged particle can penetrate, before losing all of its energy, is defined as the range in Equation (15).

$$R = \int_T^0 (-\frac{dE}{dx})^{-1} dE \tag{15}$$

Equation (14) and (15) are valid as long as the energy is sufficiently high, so the pickup of electrons by slow moving ions does not have to be taken into account.

One way of calculating the range for a particle in a material is with the software Stopping and Range of Ions in Matter (SRIM), that uses a quantum mechanical treatment of ion-atom collisions to generate tables with the projected range [13]. Figure 3 shows the range for α's and protons in silicon, obtained from SRIM. Using the software Transport of Ions in Matter (TRIM), Monte Carlo simulations makes it possible to calculate the fraction of ionization and non-ionization energy loss in the material in more detail.

Electrons and positrons also interact with the material through Coulomb scattering. When two particles of same mass collide, they may get nearly the same amount of energy and it is not possible to distinguish between them [5]. They will therefore not follow straight paths through the material and the defined range will become different from the traveled length. This makes it more difficult to calculate the energy loss of a β-particle in a material.

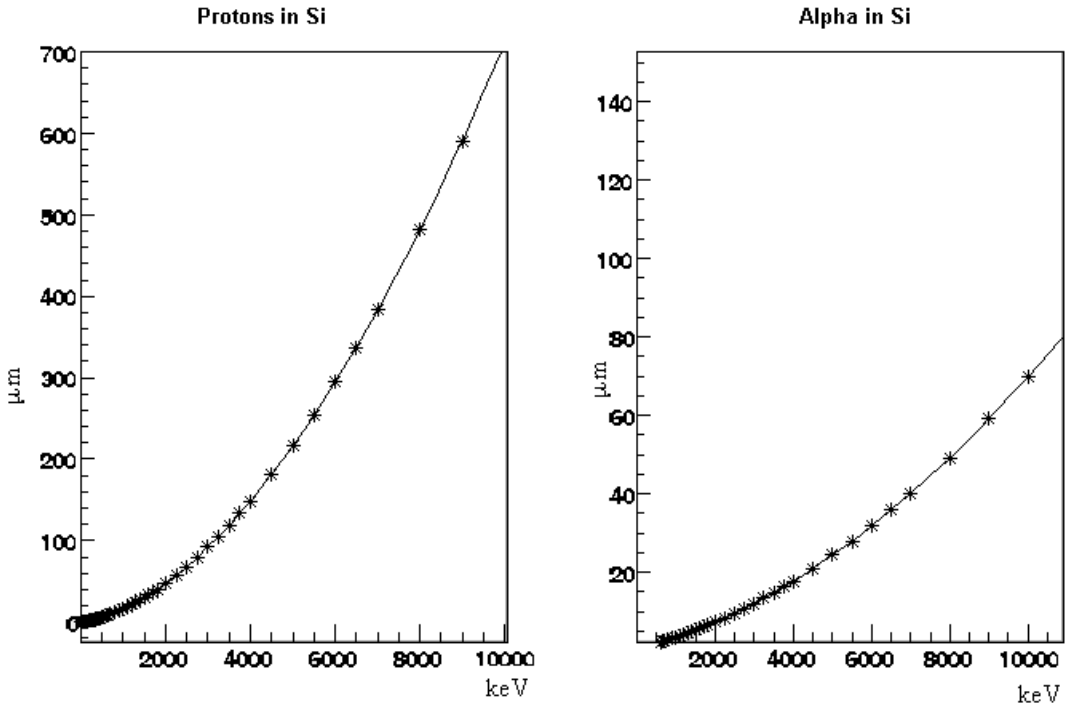

Figure 3: The range of α-particles and protons in silicon, generated by SRIM. These graphs were used for compensation of non-linear energy losses in the deadlayers of the detectors. Note that protons penetrate much deeper into the material compared to α's.

3.2 Detectors

3.2.1 Gas detectors for low-energy particles

A gas detector measures the energy loss of a charged particle through the ionization of the gas. An electric field imposed by two parallel plates at different potentials creates a drift of ions towards one of the plates and a drift of electrons towards the other plate. In the gas detector used for experiment IS507, one of those plates was a read-out grid placed in the middle of the detector.

If the electric field is sufficiently strong, the electrons drifting to the positive potential, scatter inelastically with atoms and create more ions and secondary electrons. If the gas detector operates below the *Geiger-Müller region*, the number of secondary electrons/ions is proportional to the number of primary electrons/ions and the detected energy is therefore proportional to the number of primary ionization events, and thus to the energy loss.

In the *Geiger-Müller region*, however, the detected energy is enough for total ionization of the gas and the pulse amplitude has reached its maximum. The resolution of a gas detector is in general low [5]. If a particle is not completely stopped in the gas, the resolution is coarser compared to the case with total energy deposition. The coarser resolution can be explained statistically. Assuming that the detected energy for different events are independent samples, the energy distribution due to fluctuations should follow a Poisson distribution. If the particle are totally stopped in the detector, there will be a fixed energy deposited in the detector and fluctuations cannot be treated as a Poisson distribution. The resolution is given by Equation (16),

$$R = 2.35\frac{\sqrt{Fw}}{E} \tag{16}$$

where F is the Fano factor, that takes the sample dependence into account, w is the average energy needed for ionization in the material and E is the initial energy of the particle. For the case with a Poisson distribution F is equal to 1, otherwise it is smaller than 1. Typical values of F for a gas lie in the range from 0.12 to 0.4 and w is typically in the range from 20 eV to 40 eV. This can be compared to silicon, where F is in the order of 0.12 and w is about 3.6 eV [14].

3.2.2 Silicon detectors

A silicon detector is a semiconductor that detects energy because of impinging charged particles creating electron-hole pairs in the silicon. To increase the sensitivity, a small amount of atoms with one more valence electron than the silicon can be added. The added atoms bind in the silicon lattice and provide a free electron from the covalent bond, which takes part in the drift of electrons. This is called p-doping. On the other side some atoms with less valence electrons can also be added and cause extra holes. This is called n-doping.

Between a layer of extra electrons on the p-doped side and the holes on the n-doped side, a depletion layer without free charge carriers is created. By applying a voltage, the depletion layer is increased in thickness and the current flowing through the junction is minimized. Through the interaction of a charged particle, charge-carriers (electron-holes) are created that disturbs the equilibrium and cause a direct current.

The particles lose energy in the whole volume of the detector but due to the fact that a part of the volume has to be used for read out the signal there will always be a deadlayer before the active detecting volume [5]. Often the thickness of this deadlayer is given as thickness equivalent to silicon. With known thickness of the deadlayer in a detector the energy loss before the active volume can be calculated using the graphs in Figure 3.

3.2.3 DSSSD

A Double Sided Silicon Strip Detector (DSSSD) is a thin silicon detector that consists of a certain number, N, p-doped detection strips at the front side and a certain number, M, n-doped strips at the back side. This gives $N \times M$ detecting pixels. The strips on the back side are orthogonal to the strips on the front side. By measuring the energy in the front side and the back side, in coincidence, it is possible to determine which pixel has been hit. The fact that each pixel covers only a small solid angle decreases the probability of having, for example, both one α-particle and one β-particle hitting the same pixel in the same event. That makes the DSSSD useful for reducing β-background in proton spectra [15].

3.2.4 $\Delta E - E$ detector

A $\Delta E - E$ detector consists of one thin detector that only detects a small part, ΔE, of the incident energy, backed by a thicker detector that detects the rest of the energy, E. Using the fact that different particles with the same energy lose different amount of energy in the ΔE-detector, light and heavy particles can be distinguished in a plot of ΔE against E.

3.2.5 TDC coincidences

When detecting particles from a decay in coincidence the Time-to-Digital converter (TDC) produces a signal where its amplitude is proportional to the time difference between the arrival time for two gates. The time gate for a coincidence is normally very short to minimize the possibility that gates corresponding to different decays arrive in the same event. Coincidences with particles from different decays are called accidental or random coincidences [5].

One way to see how common those accidental coincidences are, is to look at the plot of the events in coincidence in the TDC channels for two detectors, against each other. Real coincidences should correspond to a straight diagonal line as shown in Figure 4.

Accidental coincidences cause a systematic error in the measurement. The rate of accidental coincidences depends on the time resolution of the trigger. The error due to accidental coincidences is proportional to the number of events in both of the detector channels that are used for a coincidence measurement. Therefore the rate of accidental coincidences increases as the square of the rate of the decay. This leads to a necessary choice between a lower number of accidental coincidences and a lower number of observed decays. The latter, however, means an increased statistical error.

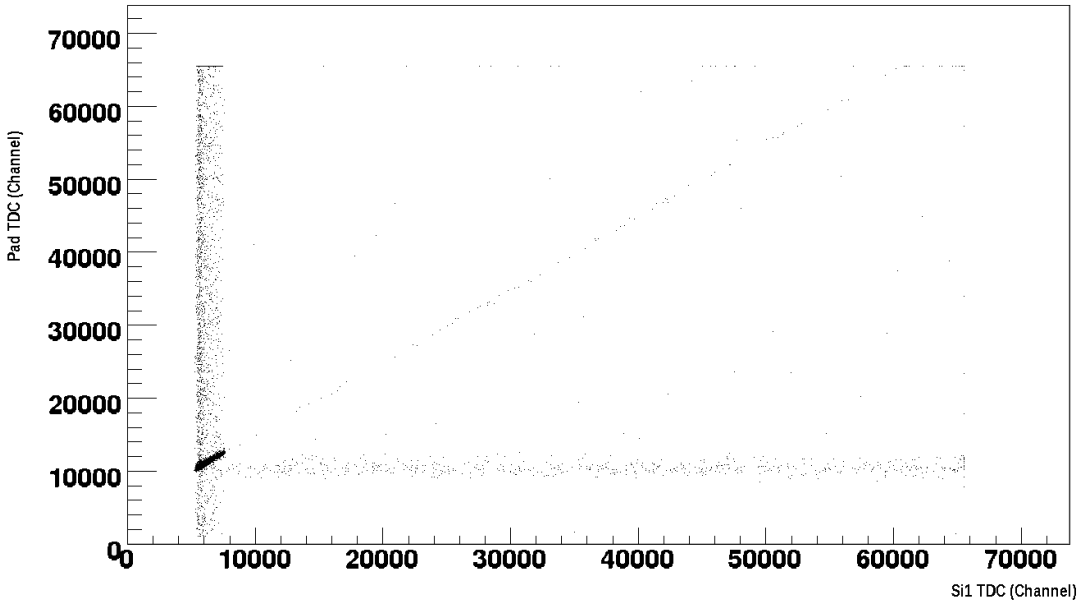

Figure 4: The detected TDC signal in the first silicon detector against the TDC signal in the silicon Epad behind the DSSSD, for events in coincidence. A real coincidence should follow a straight diagonal line. Outside this line accidental coincidences can be found.

4 The experiment

The analyzed data are from the experiment IS507 done at CERN-ISOLDE, in November 2011. Some of the data files from the experiment IS476[3] with the same setup have also been studied.

4.1 Experimental conditions

For the experiment ^{20}Mg with an energy of 60 keV was produced from a pulsed proton beam and implanted into a foil, also being the window of a gas detector. The beam of ^{20}Mg hit the foil with an incident angle of 30°, as seen in Figure 5.

Also measurements with decaying ^{21}Mg, ^{21}Na, ^{20}Na, ^{33}Ar and ^{32}Ar were made in the same way during the experiment. For calibration purposes, measurements with the α-sources ^{148}Gd, ^{239}Pu, ^{241}Am and ^{244}Cm put in front of the detectors was taken [16].

The trigger gate window for coincidence in energy signal (ADC) was 4 μs.

4.2 Beam production

To create a beam of unstable isotopes of, for example, ^{20}Mg at ISOLDE, protons are first injected in the Proton Synchrotron Booster (PSB) from the linear accelerator LINAC2. After the synchrotron the high energy protons (1.4 GeV) bombard a SiC production target. Then ionization of the atoms is done using the Resonance Ionization Laser Ion Source (RILIS). In this method resonant photon absorption is used to excite a valence electron step by step, and the ions are

[3]Done at CERN-ISOLDE in October 2011.

ionized only when the laser frequency coincides with the transition frequency of the ions, leading to a high efficiency and selectivity.

Subsequently, the ions are accelerated in an electric field before passing through the mass separator, High Resolution Separator (HRS) [17]. In the mass separator ions are deflected magnetically according to their mass-to-charge ratio, in order to minimize the fraction of other elements than the isotope of interest.

The number of protons per pulse was between $2.9 \cdot 10^{13}$ and $3.0 \cdot 10^{13}$ during the ^{20}Mg measurement [16]. In total 27.5 hours of ^{20}Mg measurements have been used in this analysis.

4.3 Detector setup

The detector setup for the IS507 experiment consisted of one gas detector filled with CF_4 gas at a pressure of 20 mbar. The foil in the gas window consisted of 1 μm polypropylene with a 400 Å thick layer of aluminum. Two circular silicon detectors, (here called Si1 and Si2), each with active thickness 300 μm, were placed inside the gas volume behind the gas detector. The deadlayers of each of those detectors were equivalent to 0.08 μm silicon.

A DSSSD detector with 16 strips at the front side and 16 at the back side was placed at the opposite side of the gas detector at a distance of 43.2 mm from the gas window. Behind the DSSSD was a quadratic silicon detector (Epad), with a thickness of 1498 μm. The deadlayer of the front- and back sides of the DSSSD are 0.1 μm and 0.8 μm in silicon, respectively. The Epad had a deadlayer of 0.8 μm. The setup with scaled distances can be seen in Figure 5.

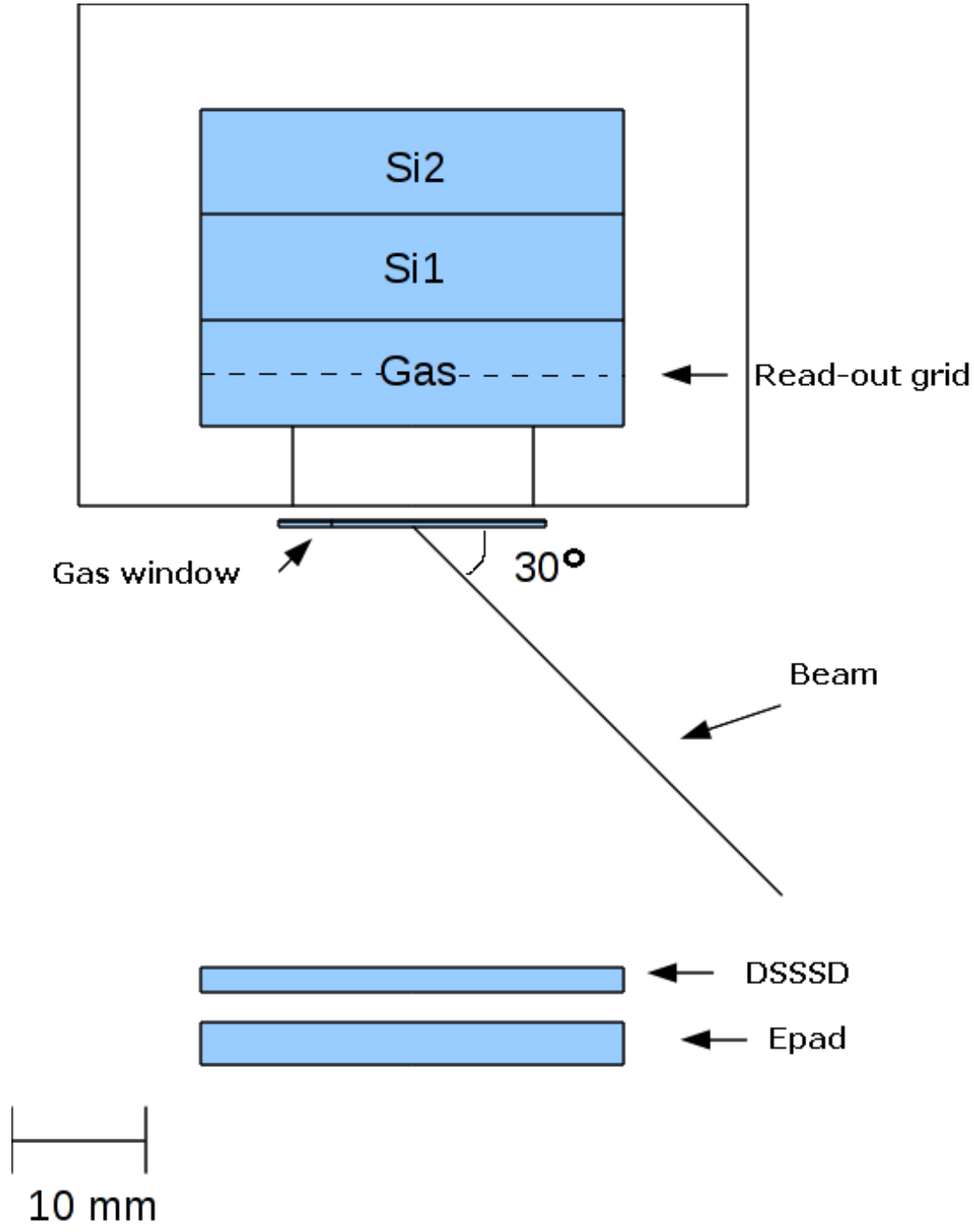

Figure 5: The detector setup used for experiment IS507 at CERN-ISOLDE. *Si1* and *Si2* are circular silicon detectors with an active thickness of 300 μm each. *Gas* is a detector filled with CF_4 gas. The DSSSD consists of 16 $\times$ 16 detecting strips, forming a pixel-grid, and has a thickness of 60 μm. Epad is a quadratic 1498 μm thick silicon detector. The decay of ^{20}Mg took place in the foil of the gas window.

5 Calibration

5.1 Unpacking

The data from the IS507 measurement was unpacked to ROOT-files with the *Unpack and Check Every Single Bit* (UCESB) unpacker [19], written by Håkan Johansson. The unpacker provides the mapping from ADC, TDC and scaler-channels. The ADC1 handled the measured energy for the DSSSD strips, ADC2 the energy for the other detectors, the TDC the time for the event in each detector channel after trigger, and the scaler channels 0 to 7 counted the number of events in each detector. Channel 8 of the scaler was used for counting of pulses generated at constant frequency, 1.2 kHz and worked as a clock. The total number of generated proton pulses was counted in channel 9 of the scaler.

After the mapping, the data from the channels was stored in n-tuples that can be handled in the C++-based software ROOT. ROOT has been developed at CERN for facilitating data analysis in the scope of particle physics [20].

An n-tuple consists of one head with several branches. The mapped channels correspond to different branches. From the head in the root tree it is possible to generate a C++-class including a template to loop over all events. This kind of loop is useful for example in matching of detected energy in the front side and back side of the DSSSD. In this data analysis the loop was also used to generate a new branch of the ROOT tree - *the time after the last beam pulse.*

5.2 Calibration of the first silicon detector (Si1)

The detected energy was assumed to be a linear function of channel for all the calibrated detectors. The calibration of the first silicon detector behind the gas detector (Si1), was made both with α-lines from ^{148}Gd (3182.68 keV), ^{239}Pu (5153.3 keV) and ^{241}Am (5485.56 keV) [1], and with known delayed proton energies from the decay of ^{33}Ar (2096.2 keV and 3171.7 keV) [21] and ^{21}Mg(1773.4 keV, 1938.7 keV and 4675 keV) [22]. The resolution was not sufficient to distinguish between the main peak of ^{239}Pu at 5157 keV and the satellite peak at 5144 keV, therefore a weighted mean value was used. The positions of the peaks were found by fitting Gaussian functions to the spectra. For ^{231}Pu and ^{241}Am a sum of two Gaussians was used. Those fits can be seen in Figure 6.

The α-sources were placed at a distance of 48.7 mm from the gas detector without any gas and without the window. The deadlayer of the Si1 detector was taken into account in the α-calibration.

Two other calibration measurements were done, one with an entrance window mounted for the gas detector but without gas and one with both the window and gas in the detector. From those measurements and obtained range curves from SRIM for α's in aluminum, polypropylene and CF_4, effective thicknesses of the foil and the gas were calculated.

By calculating the range for ^{33}Ar and ^{21}Mg at 60 keV in aluminum and polypropylene it was found that ^{33}Ar has an implantation depth equal to 57.3 nm in the aluminum and ^{21}Mg has an implantation depth equal to the whole thickness of the aluminum and 31.1 nm in the polypropylene. The effective distance from the decay to the detector was then assumed to be the mean value of the shortest distance divided by cosine, of all possible angles between 0 and the angle from the decay to the edge of the detector, weighted with the sine of this angle, to correct for the solid angle.

After compensation for the non-linear energy losses in the gas detector and the deadlayer of the Si1, a linear function between channel and energy was fitted using the least square method. Those calculations gave from ^{33}Ar a calibration of the energy detected in the detector according to Equation (17),

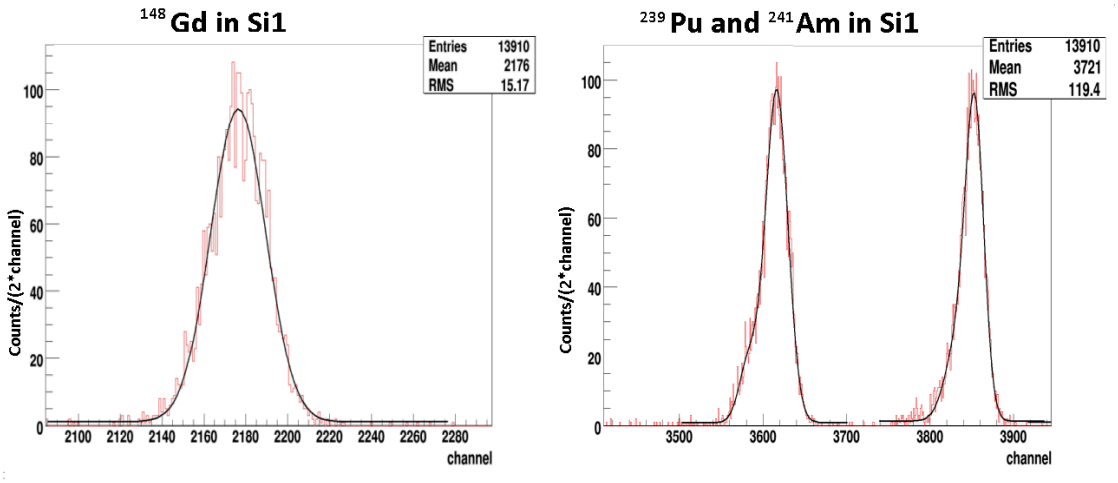

Figure 6: Gaussian fits for finding the positions of the peaks of ^{148}Gd, ^{239}Pu and ^{241}Am. For ^{239}Pu and ^{241}Am a sum of two Gaussians was fitted to take the satellite peaks into account.

$$E = 1.419 \text{ keV/channel} \cdot \text{ch} - 37.44 \text{ keV} \tag{17}$$

where ch is the channel number of the detector. From ^{21}Mg the relation is given by Equation (18).

$$E = 1.421 \text{ keV/channel} \cdot \text{ch} - 35.60 \text{ keV} \tag{18}$$

With the α-source the detected energy was found to be given by Equation (19).

$$E = 1.409 \text{ keV/channel} \cdot \text{ch} - 46.27 \text{ keV} \tag{19}$$

The estimated errors in gain and offset for calibration obtained with ^{33}Ar are $1.85{\cdot}10^{-3}$ keV/channel and 3.52 keV. With ^{21}Mg the errors are $6.3{\cdot}10^{-3}$ keV/channel and 1.33 keV, and the α-source gave errors equal to $7.99{\cdot}10^{-4}$ keV/channel and 2.69 keV.

One of the reasons why the calibration with the α-source differs in offset compared to the protons is that α's have a larger amount of non-ionizing energy loss in the silicon detector [23]. The silicon detector only detects the ionizing part of the energy loss and the detected energy for the α's is therefore smaller. By using TRIM Monte Carlo simulations the non-ionization part for protons with energy above 1000 keV was found to be about 2 keV and about 10 keV for α-particles. Below 1000 keV the TRIM simulations showed that the non-ionization part of the energy loss is a non-linear function of energy, thus those calibrations are not truly valid for lower energies.

The construction of a calibrated spectrum was done using the linear energy relations for every channel in the spectrum, followed by compensation for energy loss in foil, gas and deadlayer, calculated from the obtained range tables.

Figure 7 shows the calibrated spectrum in Si1 for ^{21}Mg protons. Fitting the 10 strongest peaks to Gaussian functions gave peak positions that differ at most 20 keV from proton energies obtained in [22]. The proton peak positions, widths (σ) and intensity for ^{20}Mg and ^{21}Mg are given in Appendix A.

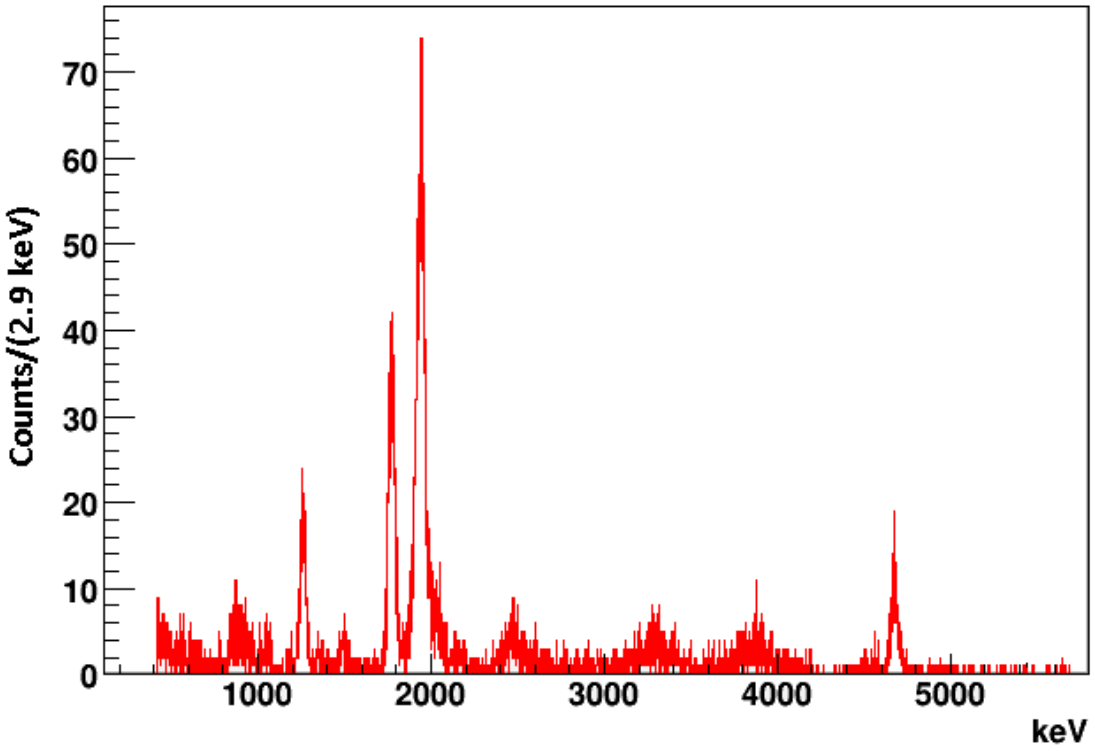

Figure 7: The calibrated proton spectrum in Si1 from the decay of ^{21}Mg. Fitting the 10 strongest peaks to Gaussian functions gave peak positions that differ at most 20 keV from proton energies obtained in [22].

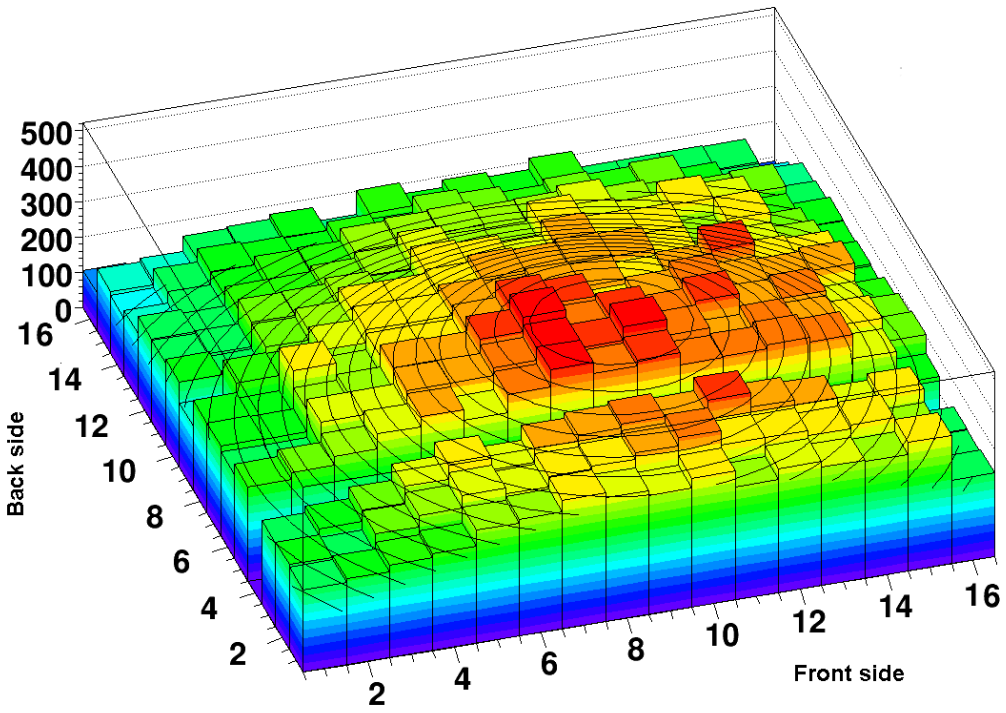

Figure 8: The distribution of protons from the decay of ^{21}Mg detected in the DSSSD. This data was fitted to a function of the closest distance from the decay to the DSSSD, in order to do the calibration strip by strip. Strip 4 on the back side did not work during the experiment.

5.3 Calibration of the DSSSD detector

The gain and offset for the different strips in the DSSSD will not necessarily be the same, therefore individual calibrations had to be done for each strip. To calibrate the DSSSD strip by strip, the effective thickness of the deadlayer for each pixel is needed. In order to get these, the angles between the decaying source and each pixel were calculated. This was done by first obtaining the shortest distance between the source and the DSSSD.

A 2D histogram with the number of hits at each pixel was created. A plot of this can be seen in Figure 8. The intensity was fitted to the probability of hitting the position (x, y), given by Equation (20),

$$P(x,y) = P_0 \frac{\cos^3\left(\arctan\left(\frac{\sqrt{(x-x_0)^2-(y-y_0)^2}}{d_0}\right)\right)}{d_0^2} \tag{20}$$

where P_0 is a dimensionless constant, d_0 is the shortest distance from the DSSSD to the source and (x_0, y_0) is the location of the closest point. The units of d_0, x_0 and y_0 were the width of strip. The same method has earlier been used by Elisabeth Tengborn in the study of *Transfer reactions in inverse kinematics at REX-ISOLDE* [24]. For the decay of ^{21}Mg, the

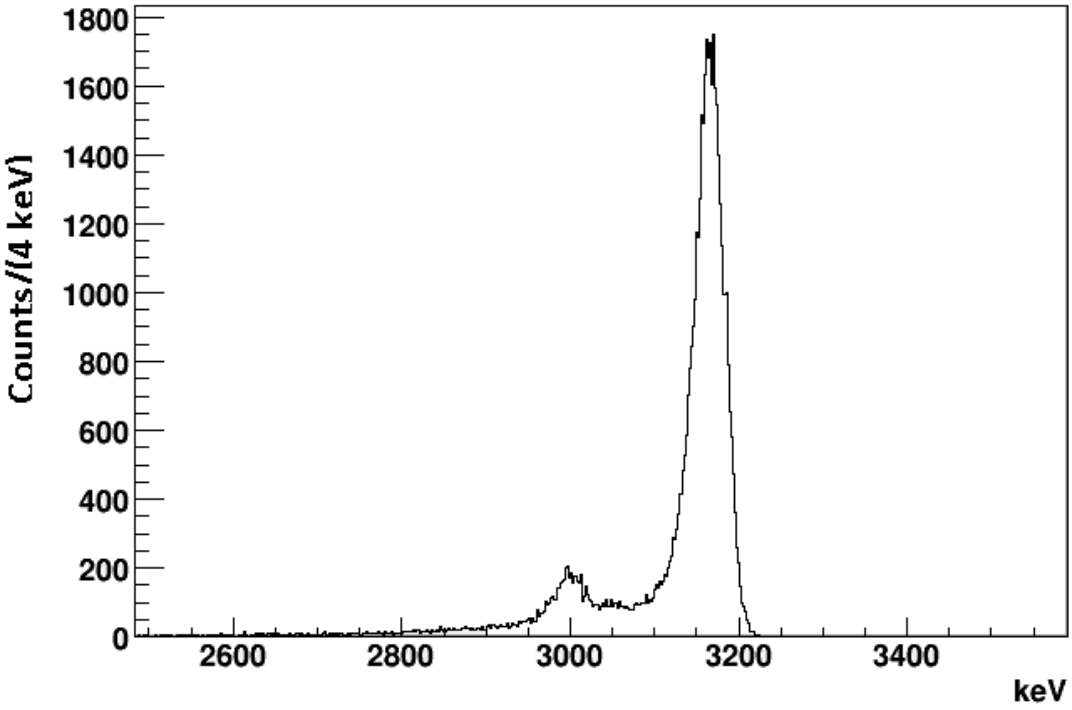

Figure 9: The detected α-energy from ^{148}Gd, in strip 1 at the front side of the DSSSD. The smaller peak is due to the read-out grid that covers 2% of the DSSSD.

shortest distance to source was calculated to be 11.256 strips and the closest point was located at strip 9 at the front side and strip 6 at the back side.

By knowing the angle to each strip the effective thickness of the deadlayer for each pixel could be calculated. The distances through deadlayer were found to be 0.107-0.139 μm for the front side and 0.860-1.010 μm for the back side. Strip 4 at the back side was a dead strip which did not work during the experiment.

For the DSSSD only ^{21}Mg contained a sufficient amount of statistics for calibration. The obtained gain for different strips varies between 1.768 keV/channel and 2.00 keV/channel and the offsets are in the interval between 187.6 keV and 299.2 keV. Gain, offset and effective thickness of the deadlayer in silicon for all strips are given in Appendix B.

The very thin deadlayer of this DSSSD is achieved through a design due to which the read-out aluminum grid cover only 2% of the detector. That reduces the deadlayer of the remaining 98% of the area, to only the implantation depth [25]. The particles hitting at the grid of the DSSSD cause a peak in the energy spectrum with lower energy than the main peak. This is shown in Figure 9, for detection of α-particles from ^{148}Gd in one strip at the front side of the DSSSD.

6 Data analysis

6.1 ^{20}Mg Spectra in the Si1 detector

The energy spectrum of all events detected in the first silicon detector, calibrated with the calibration valid for protons is shown in Figure 10.

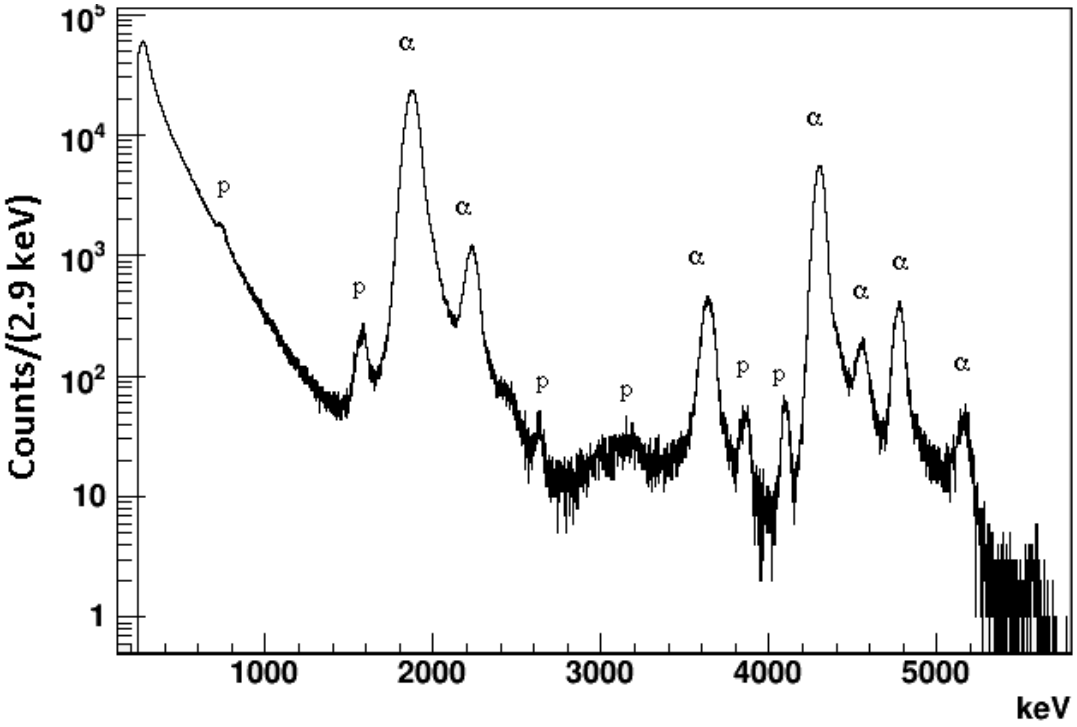

Figure 10: The energy spectrum off all detected events in the first silicon detector from the decay of ^{20}Mg. In the spectrum strong α-peaks from the decay of ^{20}Na are seen as well as a continuous distribution due to β-decay. The two strongest proton peaks can be seen around 806 keV and 1670 keV.

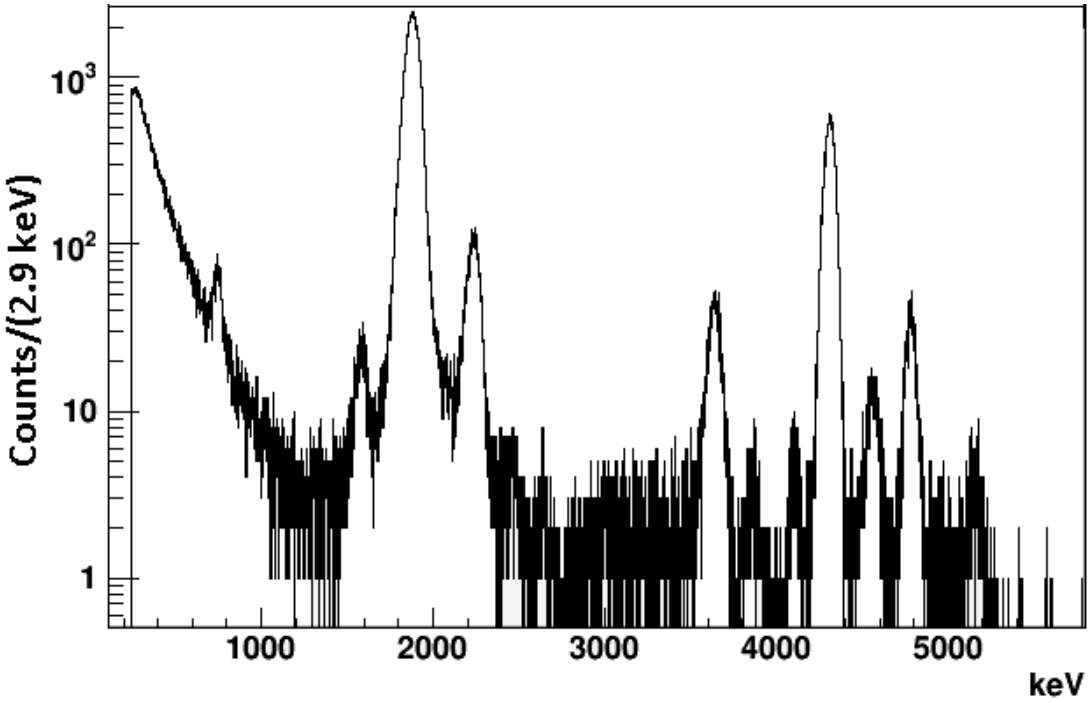

Figure 11: The energy spectrum in Si1, requiring a signal in Epad and no signal in Si2, in order to reduce the number of detected β-particles. Here α's from ^{20}Na can be seen together with the most intensive proton peaks from ^{20}Mg around 806 keV and 1670 keV. Low-energy background and electronic noise obscure any potential 450 keV protons.

In the search for 450 keV protons from ^{20}Mg decay the main challenge was to obtain proton spectra without contributions from $\beta's, \alpha's$, recoils or noise for low energies.

The thickness of the first silicon detector (Si1) is enough to stop both protons and α-particles and therefore there should only be β-particles detected in the second silicon detector (Si2). Cutting away all events with energy deposited in Si2 lowered the amount of high-energy β's in the spectrum. Since only high-energy protons or β's were detected in the Epad behind the DSSSD, an event detected in that detector was required in coincidence with Si1 and the gas detector, in order to minimize the number of β's in the spectrum of Si1. No energy condition for separating high-energy protons from β's in the Epad could be done without losing a large amount of statistics. A spectrum with a reduced number of β-particles is shown in Figure 11. In this figure α's from ^{20}Na can be seen together with the most intensive proton peaks from ^{20}Mg around 806 keV and 1670 keV. Low-energy background and noise obscure any potential 450 keV protons.

As mentioned in Section 3, the energy resolution of the gas detector is very bad compared to the used silicon detectors. The gas detector is therefore not well suited for the exact determination of particle energies. In this experiment it was used to distinguish between protons and α-particles. Since the α's lose more energy in the gas they can be identified in the plot of the detected energy from the ^{20}Mg decay in the gas detector against Si1. This can be seen in Figure 12. By plotting the spectrum from the silicon detector, excluding events with α-signature in the gas detector, a purer proton spectrum can be obtained. In this analysis, two exponential relations between the

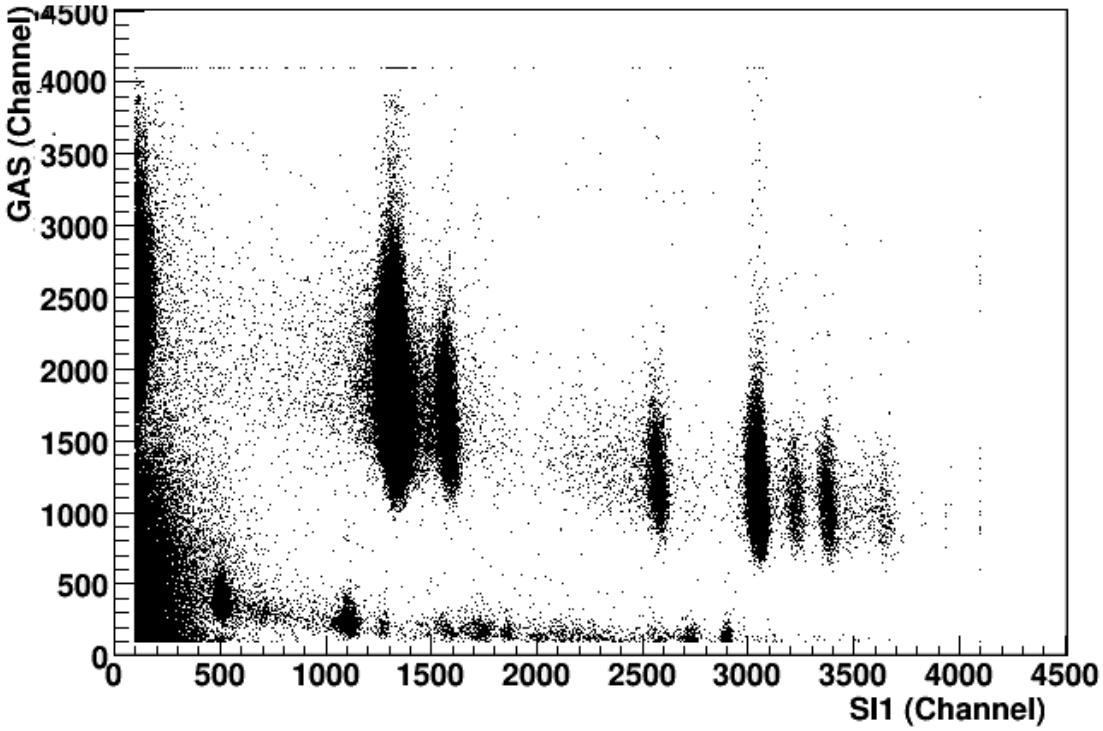

Figure 12: The raw energy deposited in the gas detector against the raw energy deposited in the first silicon detector. The α-particles lose more energy than the protons in the gas and can therefore easily be distinguished. They are here seen above channel 500 in the gas detector.

proton energy in the gas detector and the Si1 were fitted, one for a lower limit and one for higher limit. Those are shown in Figure 13.

As described in Section 4, RILIS was used for the ionization in the beam production. One advantage with this method is that, by turning the laser off, ^{20}Mg will not be ionized and a purer ^{20}Na decay can be obtained. This spectrum can be compared to the measurements with laser on, in order to identify protons and other decay products from ^{20}Mg. Na is an alkali metal with an ionization energy of 5.1 eV [26] and is therefore easier to ionize using surface ionization [27], compared to Mg with ionization energy equal to 7.6 eV [26].

Figure 14 shows the spectra for the energy in Si1 for ^{20}Mg with and without laser on. The lower plot in Figure 14 shows the ^{20}Mg spectrum after subtraction of the ^{20}Na spectrum. The ^{20}Na spectrum is scaled by a factor of $\frac{1}{15}$, in order to match the ^{20}Mg spectrum. After the subtraction, the low-energy background is still too large to identify any protons below 600 keV.

The fact that ^{20}Mg has a shorter half-life compared to ^{20}Na was used to lower the fraction of ^{20}Na decays in the spectrum. Figure 15 shows the number of identified α- and proton decay events as a function of time starting from the latest proton pulse producing ^{20}Mg. Cutting away events outside the region between 50 ms and 500 ms leads to a higher ^{20}Mg-to-^{20}Na ratio.

Further accidental coincidences were minimized by using only events with matching TDC channels, that follow straight diagonal lines in Figure 4.

The purest proton spectrum obtained in Si1, with requirements on energy in the Gas-Si1 telescope, TDC conditions on the time between Si1, Si2 and Epad and a time condition on the

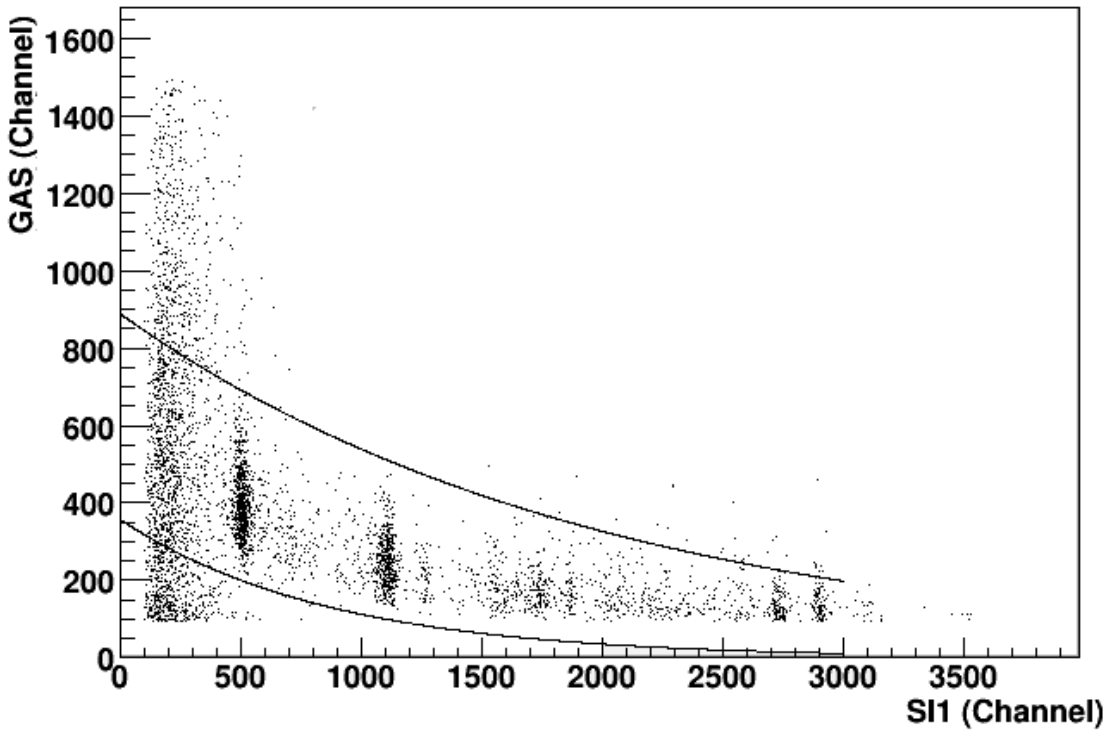

Figure 13: The raw energy deposited in the gas detector against the raw energy deposited in the first silicon detector. The picture is shown together with the exponential relations used in order to obtain purer proton spectra.

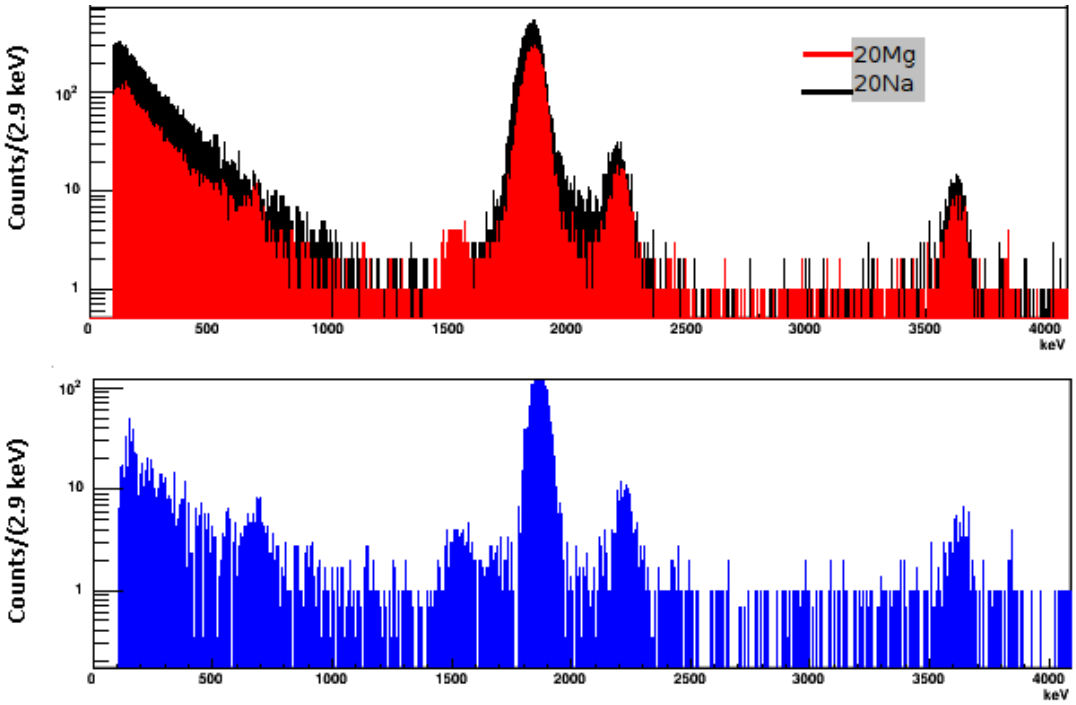

Figure 14: The upper picture shows the spectrum of the first silicon detector for measurements with ^{20}Mg and pure ^{20}Na. Proton peaks around 806 keV and 1670 keV can be seen in the ^{20}Mg spectrum. The lower picture shows the ^{20}Mg spectrum after subtraction of the ^{20}Na spectrum. The ^{20}Na spectrum is scaled by a factor of $\frac{1}{15}$, in order to match the ^{20}Mg spectrum. The low-energy background is too large to identify any protons below 600 keV.

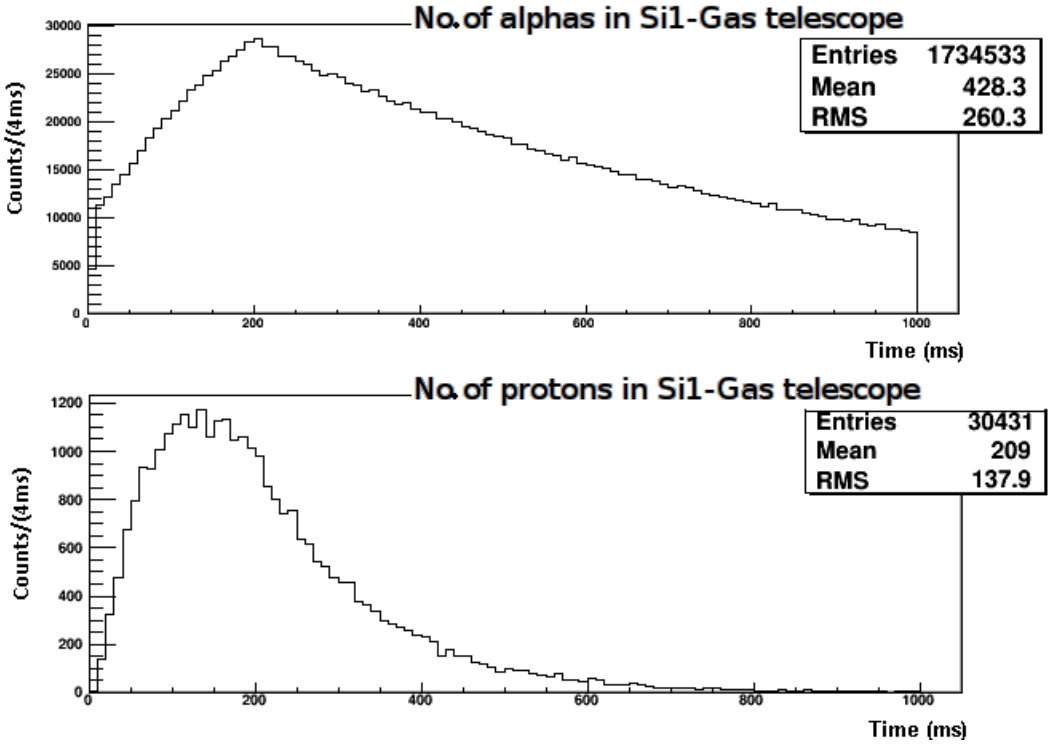

Figure 15: The number of identified α-particles in the first silicon detector (in the upper spectrum) and the number of identified protons in the same detector (in the lower spectrum), as a function of time after the latest ^{20}Mg beam pulse. The shorter half-life of ^{20}Mg compared to ^{20}Na is here reflected in the shorter time from latest beam pulse, for protons.

latest beam pulse, is shown in Figure 16.

Extracting $E_{\mathrm{ex}} - S_p$ from the found proton-lines at $E_p = 746$ keV, $E_p = 1573$ keV, $E_p = 1796$ keV, $E_p = 3861$ keV and $E_p = 4102$ keV, gives peak positions that differ with up to 36 keV compared to previous measurements [2]. The positions found in this analysis tend to be slightly lower than the previously obtained values.

Gating on a narrower interval of time after last beam pulse, reduces the statistics a lot, but also gives a higher ^{20}Mg to ^{20}Na ratio, as can be seen in Figure 15. Figure 17 shows the energy spectrum of Si1 with a time gate 70-200 ms. The amount of low-energy β-particles from the decay of ^{20}Na is strongly reduced here.

6.2 Accidental coincidences

The number of accidental coincidences was estimated by plotting the difference in TDC channels between a detected β-particle in the Si2 detector, and a detected α-particle corresponding to the most intensive α-line, in the DSSSD. Assuming that the events in the peak above the constant level of that spectrum, shown in Figure 18, are real coincidences, the proportion of accidental coincidences was estimated to be 1.46% $\pm$ 1.24%.

6.3 ^{20}Mg Spectra in the DSSSD

In the spectrum of the DSSSD, protons, α- and β-particles were seen as well as recoils of ^{16}O. Recoils were identified by looking at events in coincidence with the region for α's in the Gas-Si1 telescope.

The total energy spectrum of the ^{20}Mg decay in the front side of the DSSSD, with matched energy in the back side, for all strips, calibrated strip by strip is shown in Figure 19. In Figure 20, coincidence with the Si2 and anti-coincidence with the Epad is required, in order to lower the amount of β-particles in the DSSSD. Furthermore, only events with matching energy in both front- and backside of the DSSSD, in one pixel are added to the spectra. In total $11.85 \cdot 10^6$ events were matched and 3.46% of the events had matching energies in two pixels. Only 0.0027% of the events could be matched in more than two pixels.

After the requirements leading to the spectrum in Figure 20, $299 \cdot 10^3$ events were left. Those requirements reduced not only β's, but also protons with energy larger than 2300 keV as they are able to penetrate through the DSSSD.

In order to create the best possible proton spectra, coincidences between the DSSSD and the opposite silicon detector were studied. If an ^{16}O recoil is detected in the DSSSD the corresponding α-particle can either hit the silicon detector or escape. Identification of an α-coincidence should imply that it cannot be any proton decay in that event and the event can be removed from the spectrum.

With the DSSSD it is possible to see the position of the hit in the detector, by looking at coincidences between the front side and the back side signals. Due to momentum conservation, the ^{16}O recoil and the α-particle are emitted in opposite directions. If an α-particle is detected in the Si1, the probability of detecting a ^{16}O in the center of the DSSSD in coincidence is higher, compared to the case with a hit on the edge of the DSSSD. This is illustrated in Figure 21. An anti-coincidence between the center of the DSSSD and the Si1 should therefore, in the ideal case mean that a proton or a β-particle has been detected in the DSSSD. As the ^{16}O recoils lose all of their energy before hitting the Si1, α's corresponding to those recoils are also expected in the spectrum of the DSSSD. It can be seen in Figure 22 that the anti-coincidence requirement lowers the amount of detected α's and ^{16}O recoils and makes the proton peaks around 806 keV and 1670 keV more dominant. Since the detector efficiency is not 100%, there are still some recoils

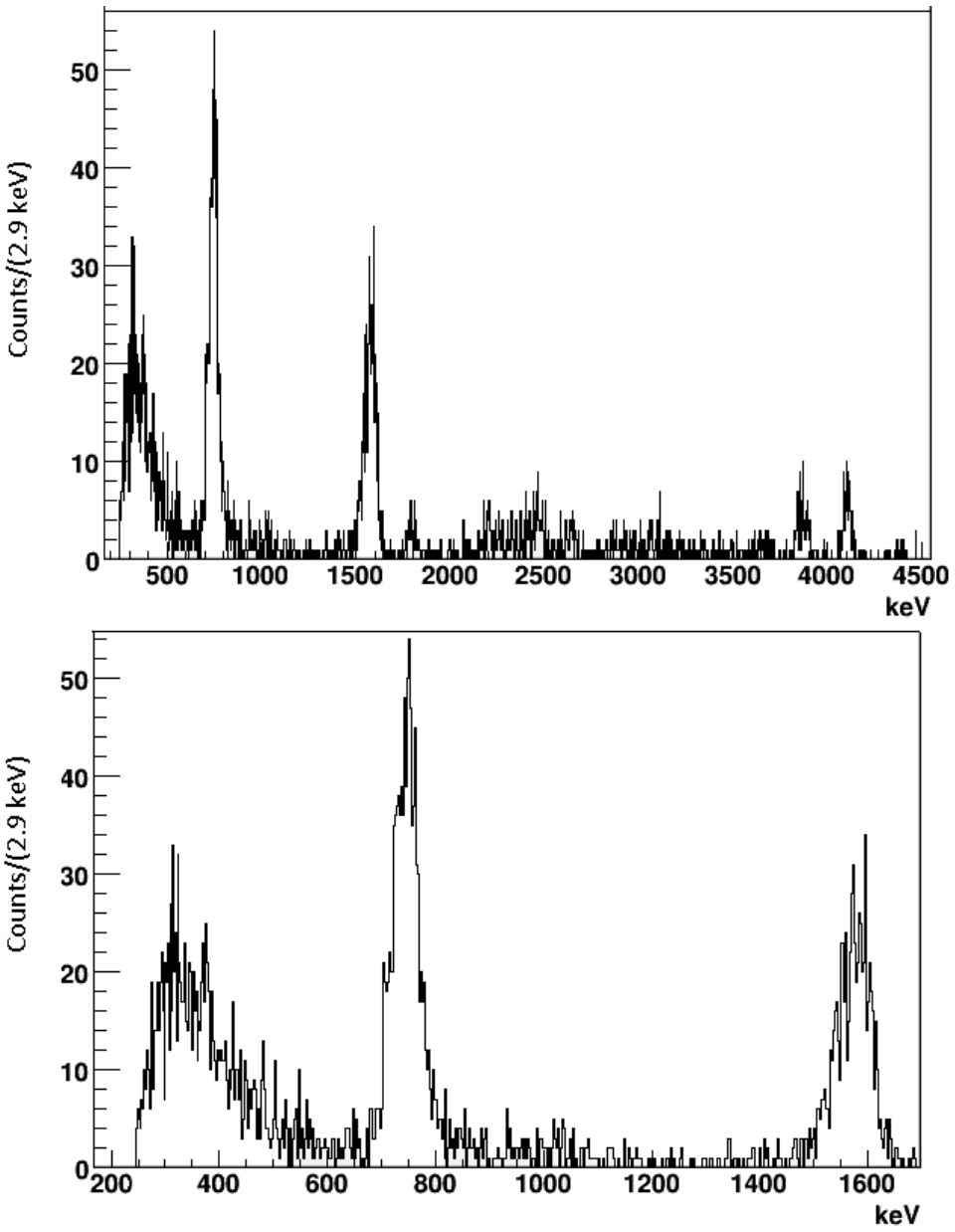

Figure 16: The purest ^{20}Mg proton spectra obtained in the Si1 detector with requirements on energy relation from the Gas-Si1 telescope, TDC relations between Si1, Si2 and Epad and time from latest beam. Peak positions are given in Appendix A and the proton energies tend to be slightly lower than previously obtained values [2]. The lower picture is a zoom that shows the low-energy region with too much β's or background for identifying any protons below 600 keV.

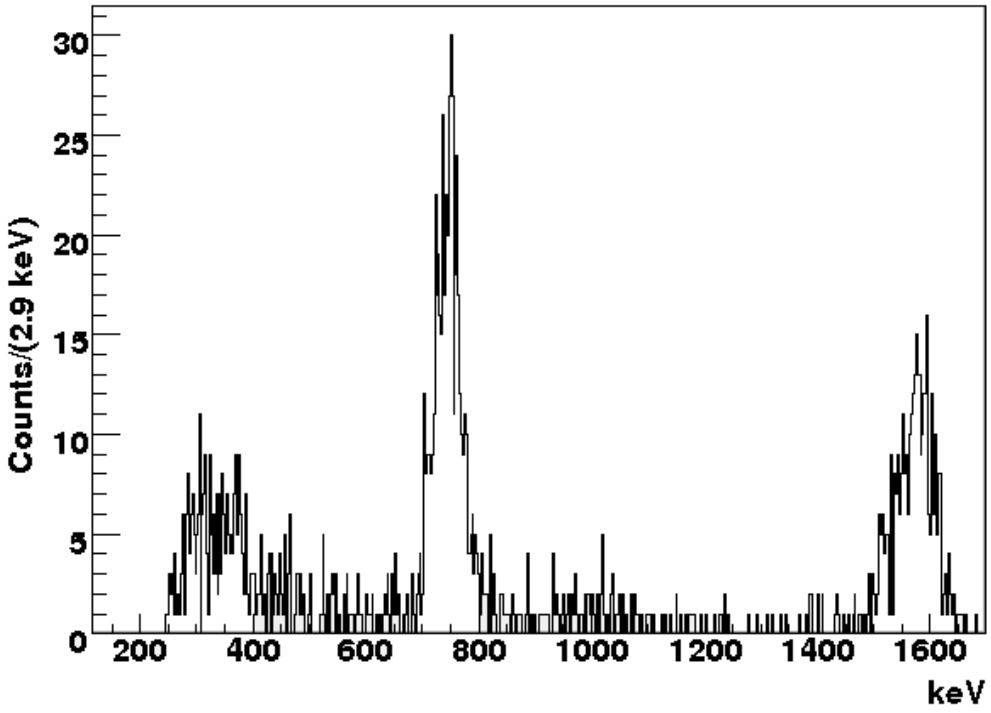

Figure 17: The ^{20}Mg proton spectrum obtained in the Si1 detector with requirements on energy relation from the Gas-Si1 telescope, TDC relations between Si1, Si2 and Epad and time from latest beam. The narrow time interval, 70-200 ms, from latest beam gives poorer statistics but higher ^{20}Mg to ^{20}Na ratio compared to the spectra in Figure 16. The amount of low-energy β-particles from the decay of ^{20}Na is therefore strongly reduced.

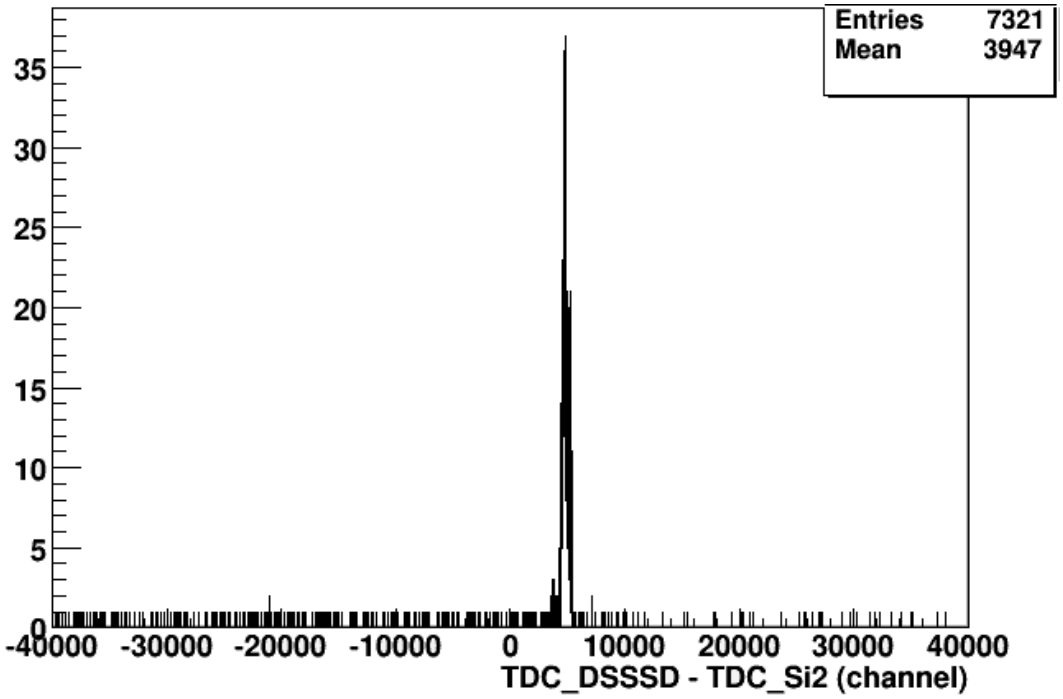

Figure 18: The number of coincidences with a β-particle in the Si2 and an α-particle in the DSSSD as a function of difference in TDC channel. From here 98.54% of the coincidences are assumed to be real coincidences located within the peak position $\pm$ 2σ (525 channels), and above the constant level. The constant level was used for estimating the number of accidental coincidences in the data.

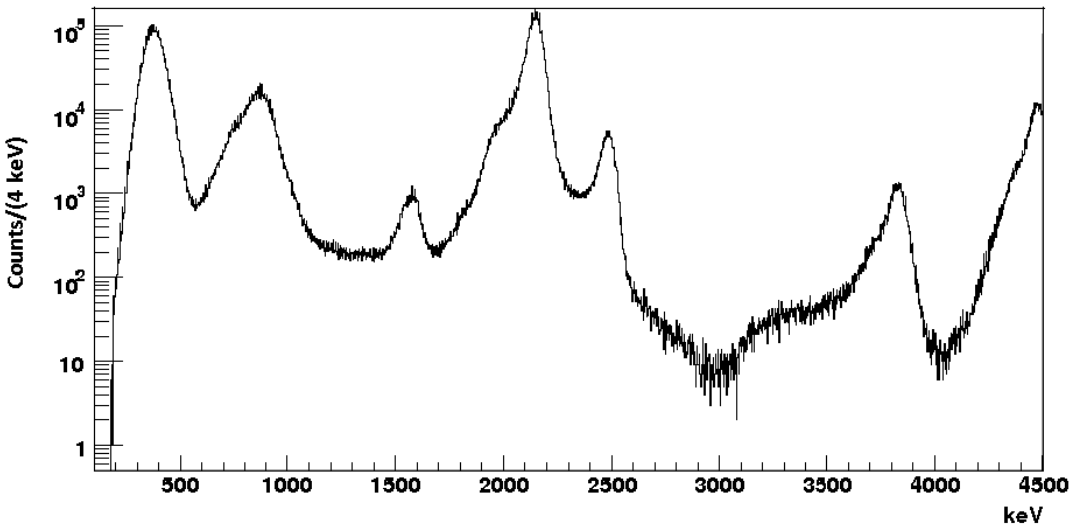

Figure 19: The ^{20}Mg energy spectrum in the front side of the DSSSD with matched energy in the back side, calibrated strip by strip.

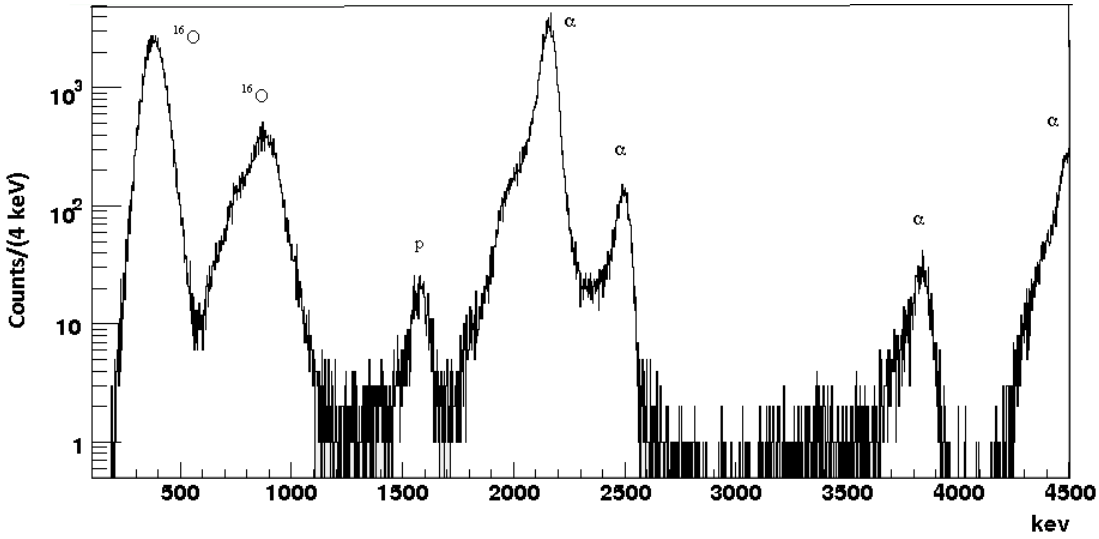

Figure 20: The energy spectrum of the DSSSD, requiring anti-coincidence with the Epad behind the DSSSD and coincidence with the Si2. Only β-particles should be detected in the Si2 and the Epad is reached by β's as well as high energy protons. Therefore the spectrum is expected to contain ^{16}O, α's and protons with energy lower than 2300 keV.

left, that together with β-background, obscure any potential protons around 450 keV. About 20% of the identified α's in the Si1 were detected in coincidence with a recoil in the DSSSD.

Studying the difference in TDC channels between the front- and back side of the DSSSD can also give an idea of what kind of particle triggered the event. From Figure 23 it can be seen that the recoils have a larger variance in Δ TDC compared to the α's and the protons. This information can be used to cut away protons from α- and recoil spectra, and give slightly purer proton spectra.

The DSSSD and the silicon detector behind the DSSSD (Epad) work as a $\Delta E - E$ telescope for protons with energy higher than 2300 keV. The detected energy in the DSSSD against the energy in the Epad for the decay of ^{20}Mg is shown in Figure 24. High-energy protons can be seen as well as α's hitting the DSSSD together with β's that reaches the Epad. Studying the β-spectrum from ^{21}Na showed that β's up to about 500 keV (calibrated for protons) could be seen in the DSSSD.

6.4 The HRS slit system

As mentioned in Section 4, the HRS was used for lowering the amount of ^{20}Na decay. In the mass separator ^{20}Mg and ^{20}Na follow different paths through the magnet, due to their slightly different masses [28]. Part of the beam can then be blocked by slits. The slit system was tested during the experiment. Three different ^{20}Mg measurements with the right slit placed at 2.6, 2.2 and 2.0 were done during 42 to 47 minutes. Gating on the most intense proton peak and the most intense α-peak in Si1 gave a proton to α ratio equal to 0.0081 for the right slit at position 2.6, 0.0123 for 2.2 and 0.0147 for 2.0. From position 2.6 to 2.0 the ratio was improved by 81%. This change lowered the total number of detected protons by 62%.

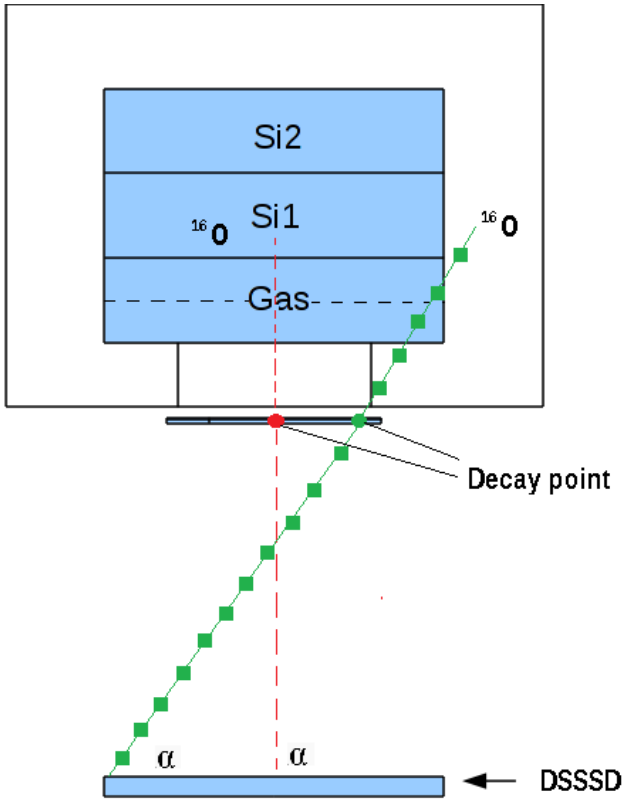

Figure 21: Due to momentum conservation the α-particle and the ^{16}O recoil are emitted in opposite directions. The red line shows a coincidence between the center of the DSSSD and the Si1. The green line (with squares) shows an α-particle detected in the DSSSD and an escaping ^{16}O.

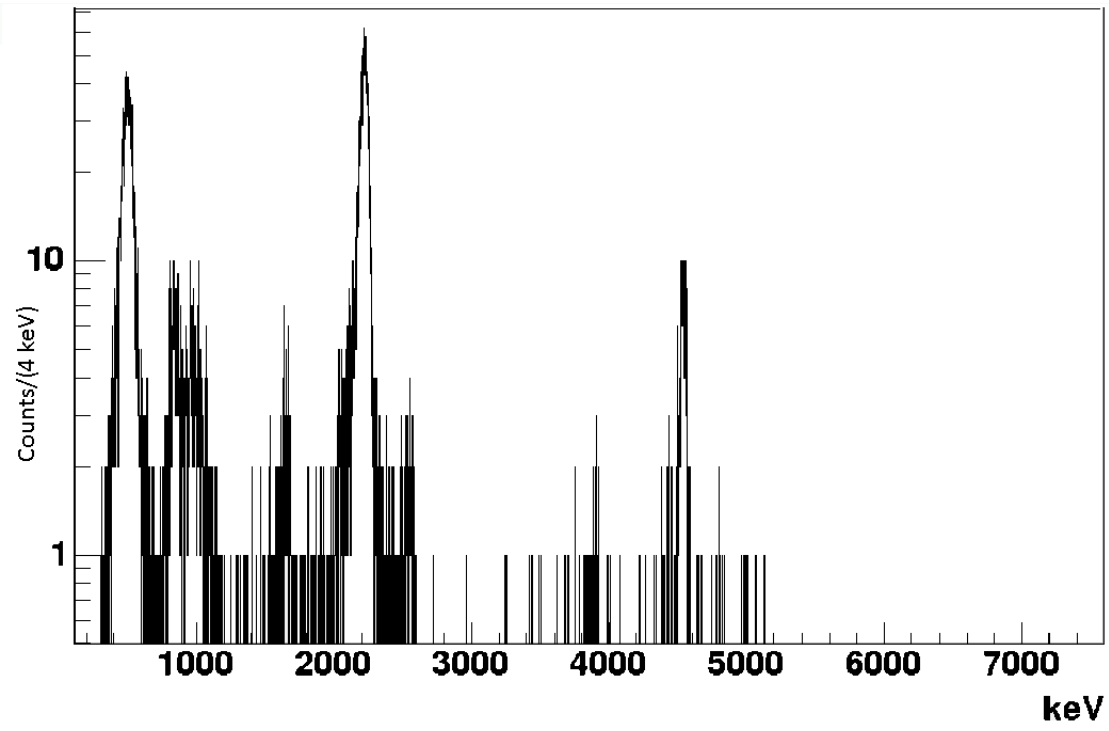

Figure 22: The ^{20}Mg energy spectrum in the DSSSD with required anti-coincidence with the gas and the first silicon detector. The proton peaks around 806 keV and 1670 keV can be seen, but lower protons are hidden in recoils and β-background.

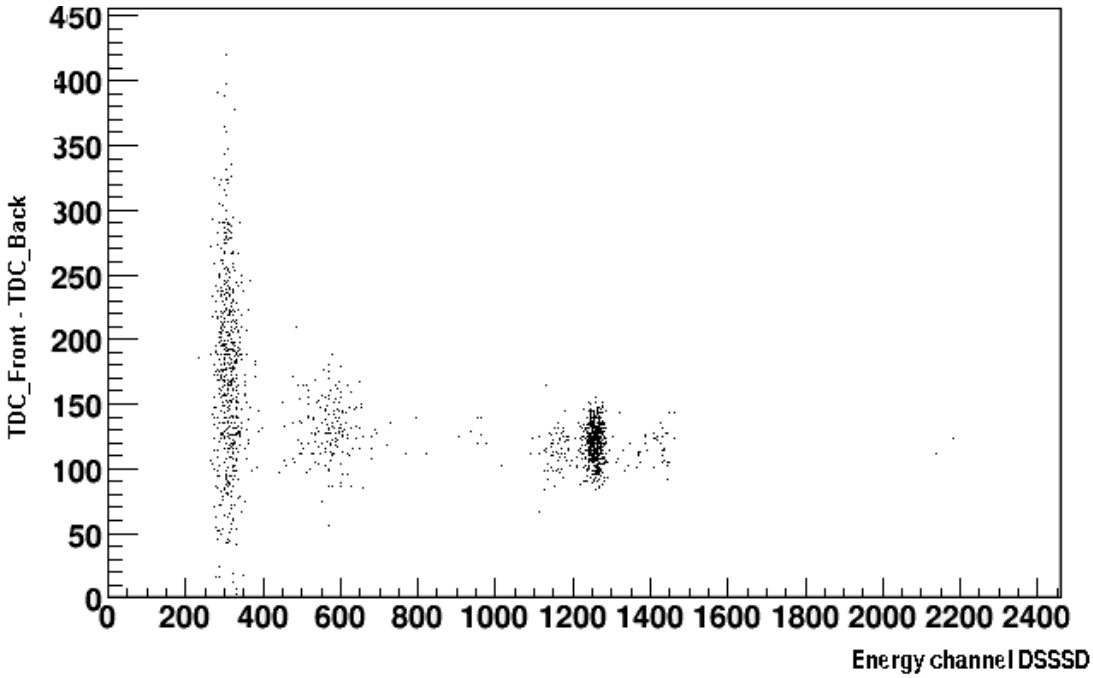

Figure 23: The plot shows the TDC channel in the front side minus the TDC channel in the back side of the DSSSD, versus the energy deposited in the front side of the DSSSD. Around energy channel 300 in the DSSSD, where recoils are expected, the variance in Δ TDC is large. The protons around energy channel 950 show a small variance in Δ TDC. This plot is obtained with required signal in the second silicon detector (Si2) behind the first Gas-Si1 telescope and is therefore not expected to contain much β's in the DSSSD. The Δ TDC information can be used to obtain purer α-spectra, and slightly purer proton spectra.

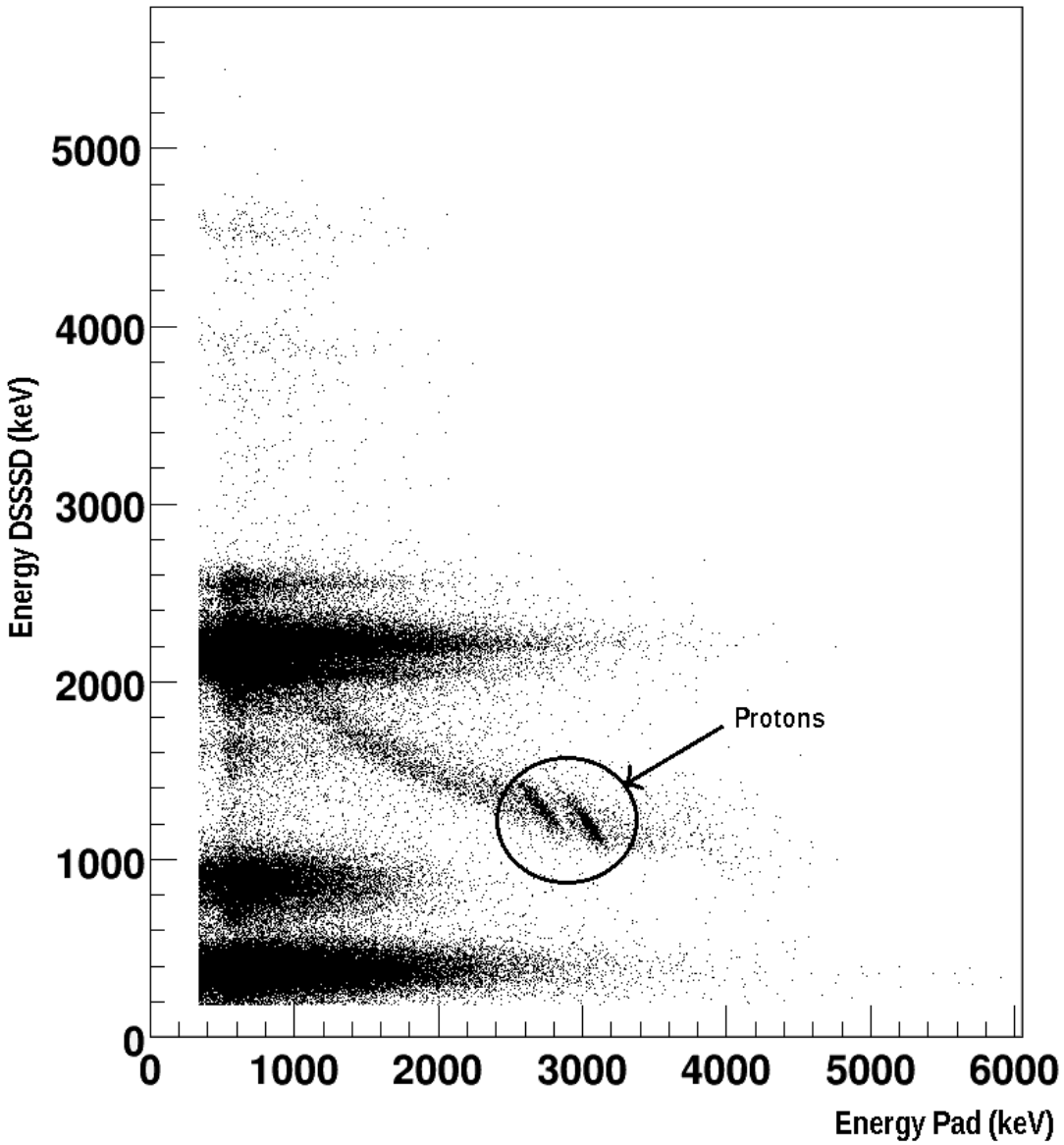

Figure 24: The $\Delta E - E$ plot of the DSSSD and the Epad, for ^{20}Mg measurements. High-energy protons can be seen around 3000 keV in the Epad and 1400 keV in the DSSSD. Also α's hitting the DSSSD together with a β-particle that reaches the Epad are seen.

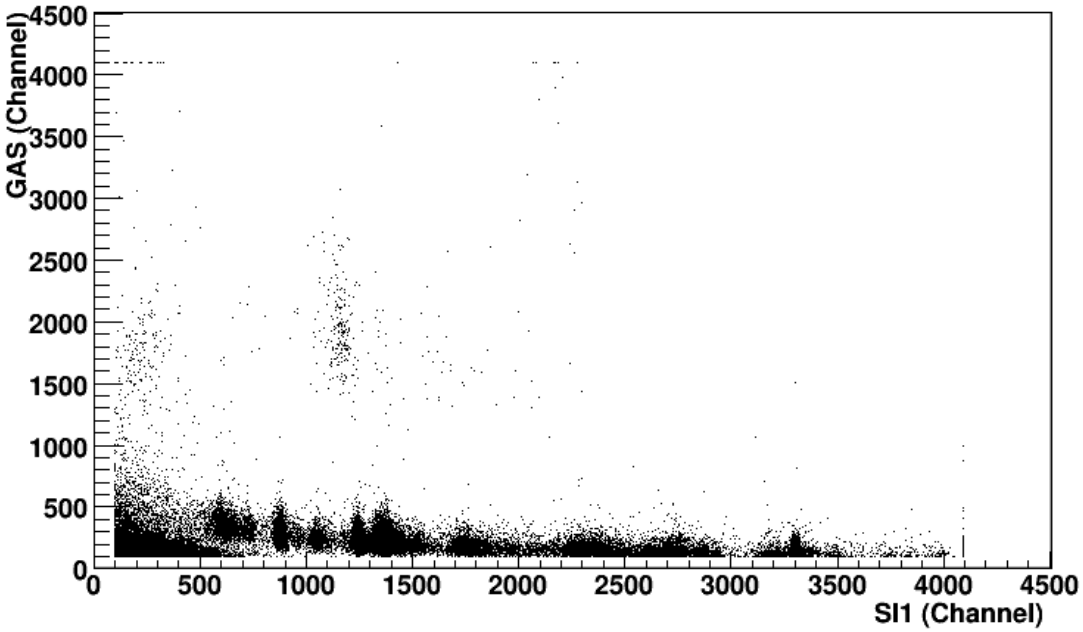

Figure 25: The raw $\Delta E - E$ plot of the Gas and Si1 detector for measurement with ^{21}Mg. Above the protons and around channel 1200 in Si1, α's that probably originate from β-delayed α-emission to ^{17}F, are seen.

6.5 β-delayed α-emission in ^{21}Mg

The isotope ^{21}Mg, that was used for the calibration of the detector has a 32.6% decay probability via β-delayed proton emission. An upper limit of the β-delayed α-emission to ^{17}F has previously been found to be 0.5% [1]. The lowest existed state in ^{21}Na with spin corresponding to allowed decay from ^{21}Mg and with excitation energy above the threshold for (^{17}F+α), exceeds the threshold by 2410 keV [1].

Above the protons in a $\Delta E - E$ plot of the Gas and Si1 detector, events with α-calibrated energy equal to 1913 keV were found. The $\Delta E - E$ plot is shown in Figure 25. The intensity of this peak compared to the intensity of the main proton peak is 1 : 61.8. The intensity of the second strongest proton peak is 1 : 2.17 compared to the main peak. Assuming the main proton peak having a branching ratio equal to 10.45% [22], gives a 0.169% branching ratio to the state in ^{21}Na corresponding to this α-emission.

The potential α-peak is not coincident with events in the DSSSD, which means that the corresponding ^{17}F could not be detected. No events were found at the same position in the $\Delta E - E$ plot of Gas and Si1 with pure ^{21}Na measurement, which strongly indicates that these events are α's from ^{21}Mg decay.

Further, the half-life of the α's seems to be similar to the half-life of the protons from ^{21}Mg. In Figure 26 the time from latest beam pulse is shown for the decay of ^{21}Mg. The upper picture is with proton gate in the Gas-Si1 telescope and the lower one is with α-gate.

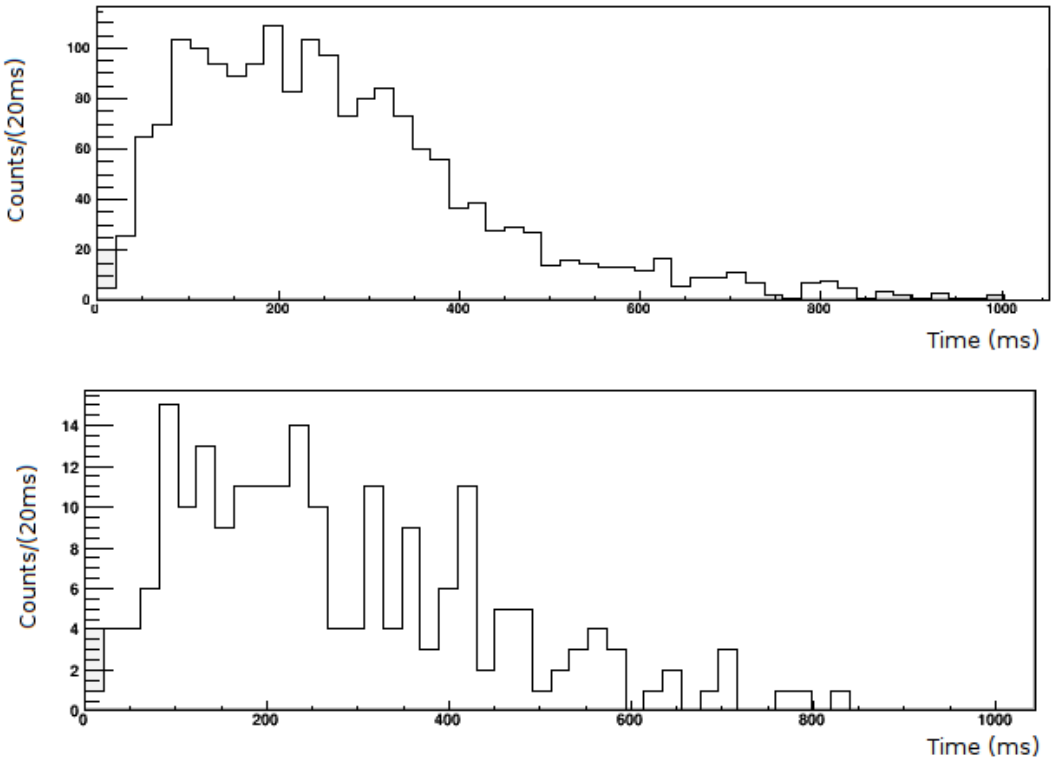

Figure 26: The time after latest beam pulse for the decay of ^{21}Mg. The upper picture is with proton gate in the Gas-Si1 telescope and the lower one is with α-gate in the same detector.

7 Simulations

7.1 The IS507 setup

The software package GEANT3 was used for simulation of the energy deposition of the particles in the detectors. GEANT3 has been developed at CERN and uses the Monte Carlo simulation technique to describe the passage of particles through matter [29]. The simulation of the IS507 setup starts with an isotropic β-decay of ^{24}Mg[4] 0.05 μm inside a 1 μm thick, 12 $\times$ 12 mm foil of polypropylene. In positive z-direction 2 mm passive gas is followed by 2 mm active gas and 2 mm passive gas. After the gas, two silicon detectors, each 300 μm thick, are placed. In the negative z-direction, at 44.4 mm, a 60 μm thick silicon detector with area 48 $\times$ 48 mm is placed (DSSSD), backed by a 1500 μm thick silicon detector (Epad).

The β-decay is followed by either an α-particle with an energy of 2.48 MeV (probability 11.25%) or 4.43 MeV (probability 3.75%), an ^{16}O with 0.54 MeV (probability 11.25%) or 1.11 MeV (probability 3.75%), or a proton with energy 0.45 MeV (probability 0.18%), 0.8 MeV (probability 0.38%) or 1.67 MeV (probability 0.19%). The α-particles and the recoils of ^{16}O were not simulated in coincidence. In total $7 \cdot 10^6$ events were simulated.

Figure 27 shows the energy spectrum of the simulated data in the first silicon detector (Si1) without any cuts. Compared to the real spectrum the 806 keV proton peak is easier to see, but the 450 keV proton-line is hidden in β's. Figure 28 shows the $\Delta E - E$ plot of the active gas and Si1, first without any cuts, then with detected signal in the Epad and no signal in Si2. As there are no accidental coincidences, other background or electronic noise in the simulated data, it is easy to see the proton- and α-lines.

The spectrum of the simulated data obtained for the DSSSD is shown in Figure 29. In the simulated data the 450 keV proton peak can easily be seen and most of the recoils are stopped in the implantation foil. Low-energy β's are present up to about 800 keV.

Figure 30 shows the spectra of the Si and DSSSD with different coincidence requirements for lowering the β-background. From this, it can be seen that also without accidental coincidences it is not possible to find the 450 keV proton-line in the Si1 spectrum. Without any ^{16}O recoils hitting the DSSSD and a very thin deadlayer of the DSSSD, this simulation shows that it should be possible to observe the 450 kev proton-line in the DSSSD, but in reality the deadlayer was too thin to stop the majority of the recoils.

7.2 Thinner detectors

From the ^{21}Na measurement it was seen that β's up to about 500 keV could be detected in 60 μm silicon. With a thinner detector this limit can hopefully be put below the energy of the interesting 450 keV protons. One existing very thin detector is the 1 μm thick R310 monolithic silicon detector telescope from SGS-Thomson [30]. The ΔE detector is backed by a 400 μm thick silicon detector. This detector has a deadlayer of 1 μm silicon, that together with the ΔE can stop the recoils from ^{16}O, before reaching the E-detector. The active area of the detector is 3.5 $\times$ 3.5 mm. Figure 31 shows the simulated data in a $\Delta E - E$ plot for this detector placed at a distance of 1 mm from the source.

The simulated decay is the same as for the simulation of the energy detection of the setup used for IS507, but the probability of 450 keV proton emission is lowered to 1.1%, and 1% random β's are added. From this simulation β-particles seems to be a problem up to about 100 keV in

[4]Because ^{20}Mg was not on the list of possible simulation ions in GEANT3, ^{24}Mg was used with the qvalue for β^+-decay of ^{20}Mg (10 MeV).

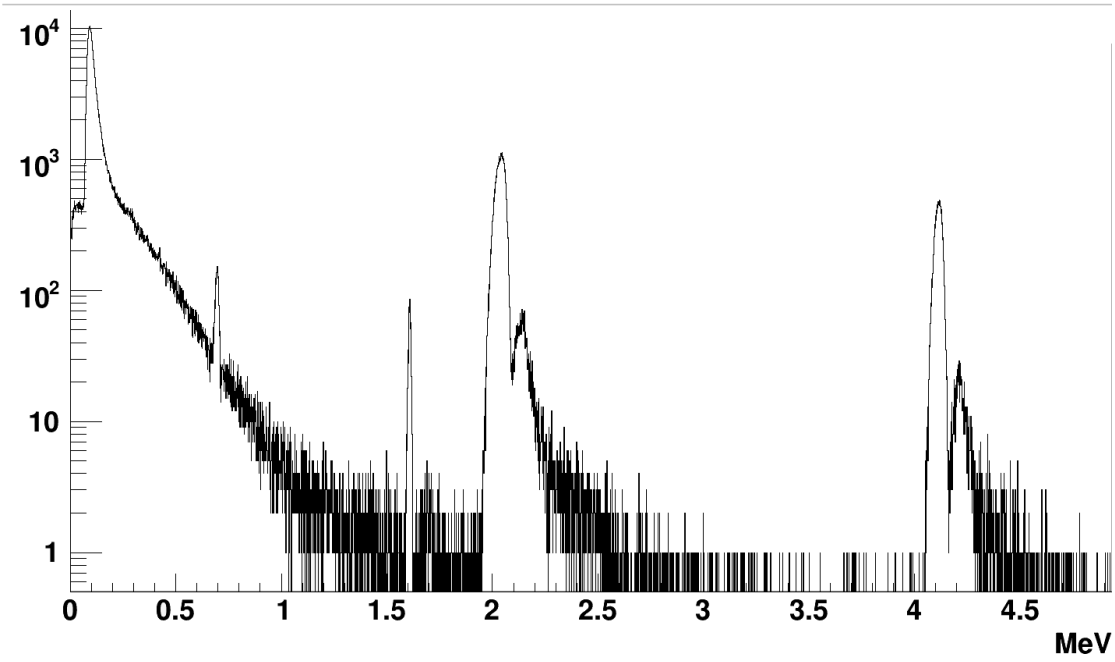

Figure 27: Energy spectrum of simulated data detected in Si1 from GEANT3, without cuts.

the ΔE detector, but after deadlayer and ΔE detector, 450 keV protons have only about 200 keV and they mix with the β-background.

The simulations show that the problem with β-particles becomes larger with decreased distance to the implantation point, but with larger distance the probability of detecting a particle in coincidence with a β-particle in a detector placed on the opposite side, is reduced. With one detector, 1 mm from the implantation point and the Si2 at the same position as during the IS507 experiment, 1.5% of the simulated events were detected as coincidence of those two detectors. In the simulation with the IS507 setup, 0.44% of all simulated events were detected in coincidence with the DSSSD and Si2. It should be noted that the solid angle covered 44.4 mm from the implantation point is only 0.05% of the angle covered at distance 1 mm.

It is also important to note that the real β-spectra look different from the simulated ones. One reason is that the simulation has no energy threshold at 200 keV, like the real DSSSD. The other is that the real spectra are shown calibrated with a calibration which is valid for protons but not for β's. The fact that GEANT3 is designed for higher energy simulation may increase the error in the studied low-energy region.

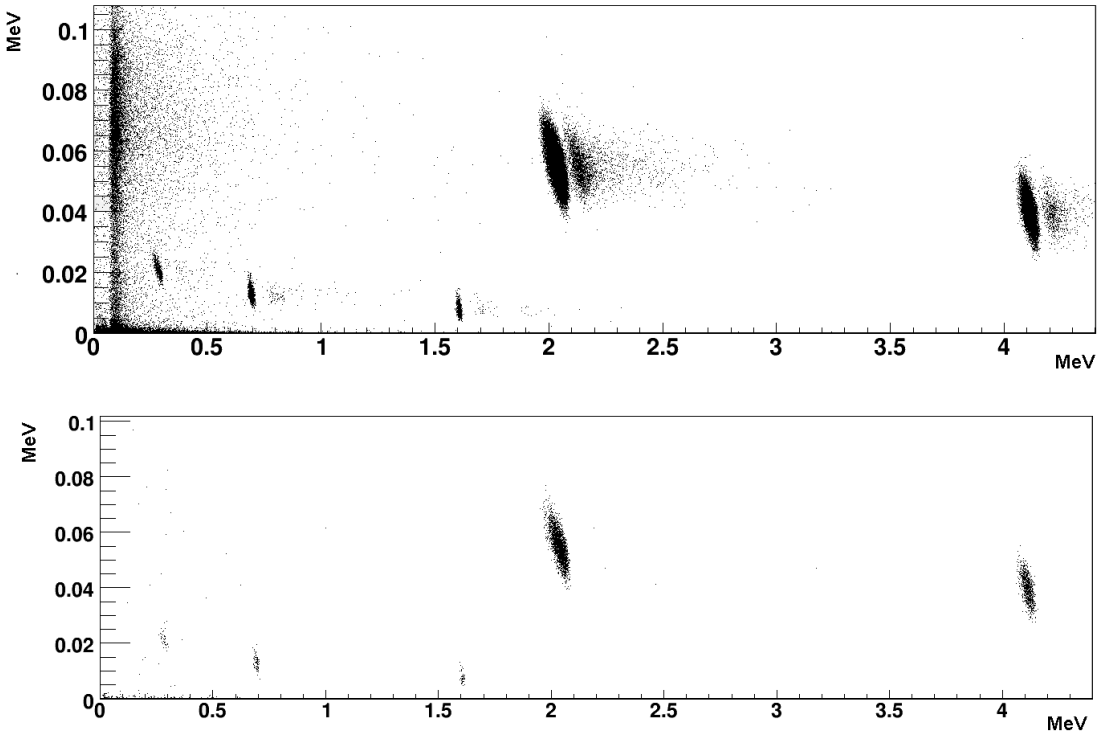

Figure 28: Energy spectra of simulated data from GEANT3, active gas detector against Si1. The upper picture is without cuts, and the lower requires a detected signal in the Epad and no signal in Si2.

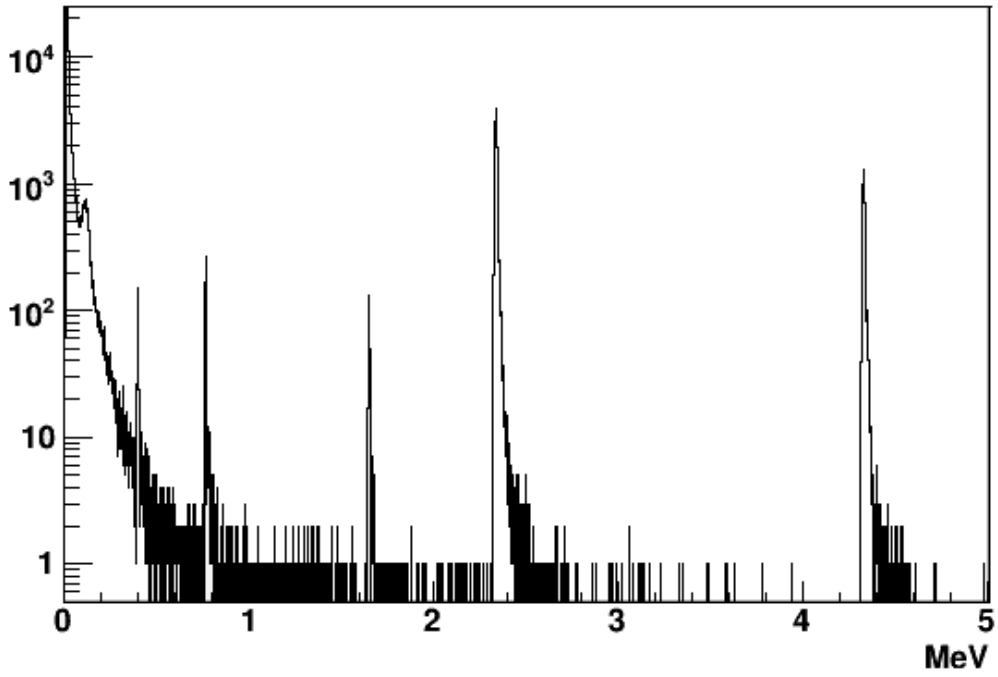

Figure 29: Energy spectrum of events detected in the DSSSD, simulated with GEANT3, without cuts.

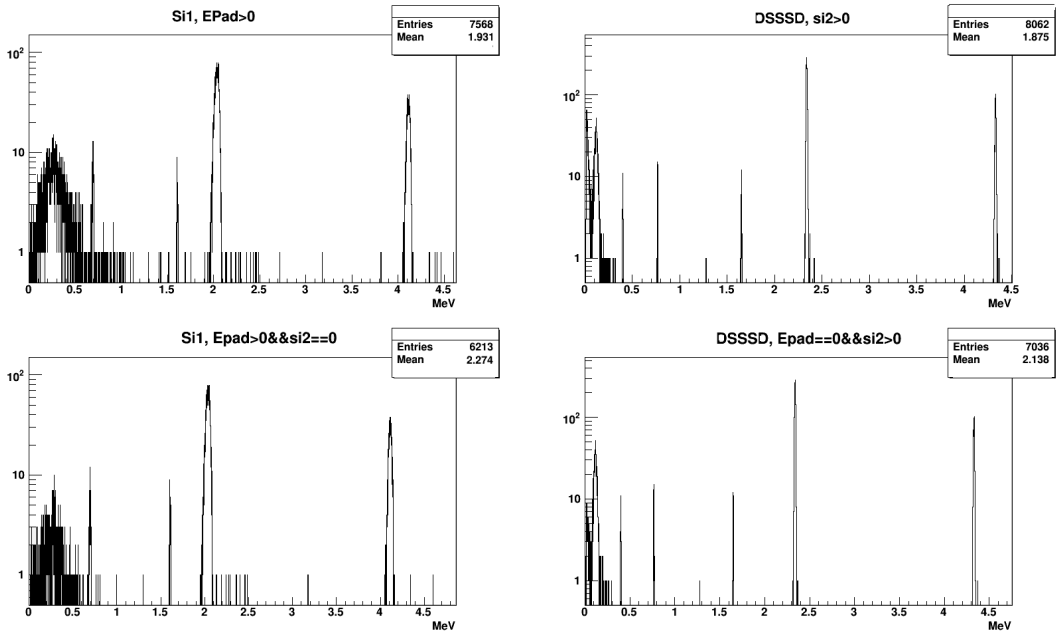

Figure 30: Energy spectra of simulated data detected in Si1 and DSSSD, requiring coincidences with the opposite side. In the Si1, the 450 keV protons cannot be observed, but excluding recoils in the DSSSD, a proton peak at 450 keV is visible.

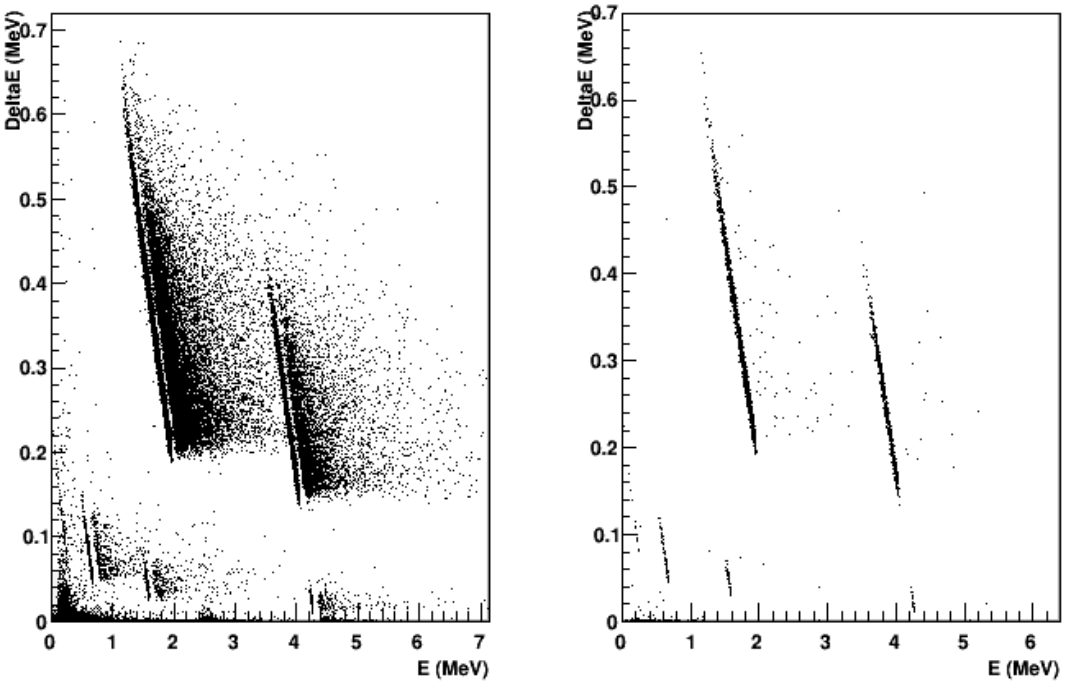

Figure 31: A $\Delta E - E$ plot of ^{20}Mg decay detected by a 1 μm thick ΔE detector, simulated in GEANT3. To the left, the simulation with detected α-particles, protons and β-particles, is shown. To the right the β-particles have been detected in another detector placed at 180° with respect to the $\Delta E - E$ telescope.

8 Results

The best obtained ^{20}Mg proton spectra from the Si1 detector are presented in Figures 16 and 17. In the spectra shown in Figure 16, 8302 events are found and the number of events in the main peak within a width of $\pm 2\sigma$ (103.6 keV) is 965. The peak around 1600 keV, within $\pm 2\sigma$ (120.4 keV) contains 627 events. In a region with a width of 103.6 keV, around the expected position of the 450 keV protons, 452 events can be found. Assuming that the 806 keV peak has a decay probability of 11.5%, the only limit for the 450 keV protons is that they are less than 5.39%, which is far larger than the previous measured value 0.1%.

In the spectrum shown in Figure 17, 2078 events are found. In this spectrum, with reduced amount of β-particles, the same analysis gives an upper limit of 2.78% proton decay to the 2645 keV state in ^{20}Na.

Due to the problems with recoils from ^{16}O in the DSSSD, no low-energy protons could be seen or analyzed in that detector.

8.1 Errors

8.1.1 Resolution

To estimate the errors in the energy spectra the Full Width at Half Maximum (FWHM) resolution has been used. The width of the α-peak from ^{148}Gd at half intensity was measured to be 57 keV in the Si1 detector and on average 38 keV for individual strips in the DSSSD (for the main peak with thin deadlayer, seen in Figure 9). Looking at the sum of all strips in the DSSSD the width is 171 keV, which confirms the importance of the calibration strip by strip. The statistical error of the mean value of the fitted Gaussian functions, used to find the peak position in Si1, was calculated from the σ of the Gaussian to be 0.34 keV. This is negligible compared to other errors.

In the simulations, no widening to model the resolution of the detectors have been performed.

8.1.2 Background spectra

Background in the detectors from events not caused by implanted ^{20}Mg is another important source of error in the analysis. During the experiment measurements with closed beam gate were done for 86 minutes, 12 minutes after the ^{20}Mg beam was switched off. In this measurement 307 events were detected in Si1 and the spectrum is shown in Figure 32. Figure 33 shows the location of the background events in a $\Delta E - E$ plot of the Gas and Si1 detector. It was found that 70% of the detected events are located at energies lower than 700 keV in the Si1 and below channel 1000 in the gas detector, thereby disturbing the identification of low-energy protons.

The high energy background has the same energy as α's from ^{148}Gd and is likely due to contamination on the implantation foil. The origin of the low-energy background is more uncertain.

Assuming a constant rate of low-energy background during the whole experiment should give 4106 low-energy background events in the spectrum shown in Figure 10. This is equal to 0.05% of all events in the energy region below 700 keV in Si1 and below channel 1000 in Gas. After all other cuts used it is not straight forward to calculate the remaining number of background events. Most of the background is not in coincidence with the Epad, but during the ^{20}Mg measurement, background events might coincide with β's from the decay in the Epad.

In the spectrum shown in Figure 16, about 65% of the measuring time is gated on the time passed since last beam pulse. That means that 9.5 hours are left, which in the worst case gives 1437 events as low-energy background. This is 23% of all detected events in that energy region.

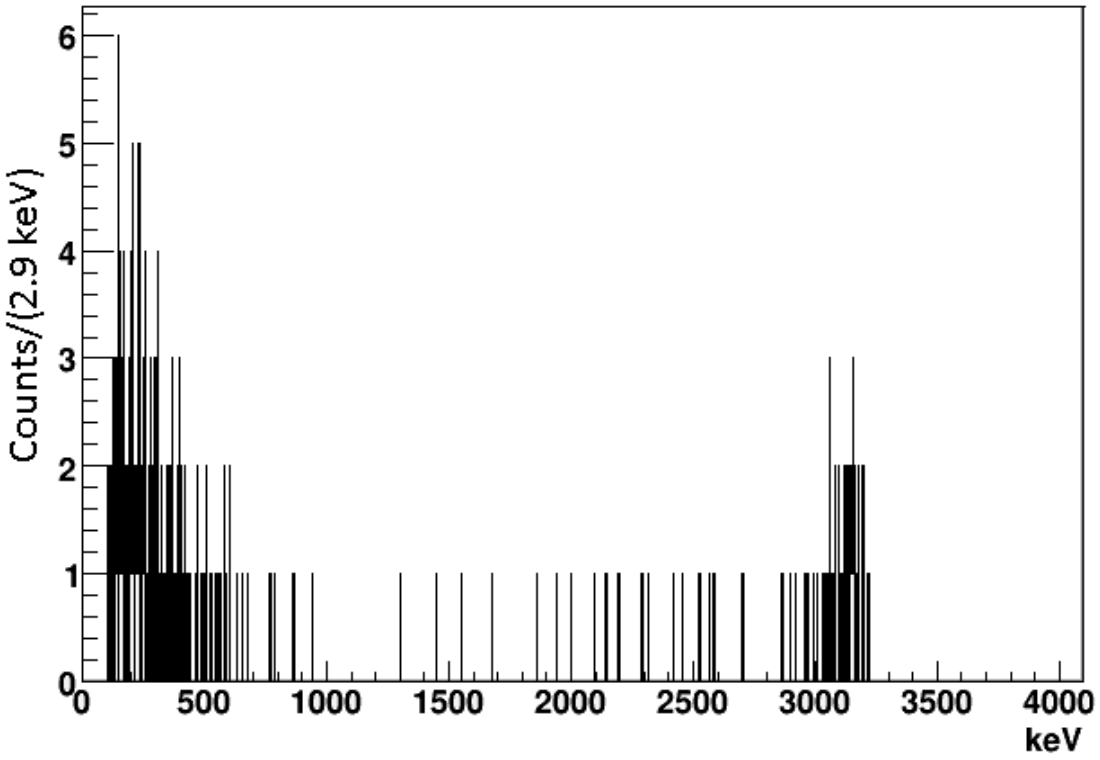

Figure 32: The background spectrum obtained for Si1, after 86 minutes of measurement with closed beam gate. Here 307 events were detected, 214 have an energy lower than 700 keV.

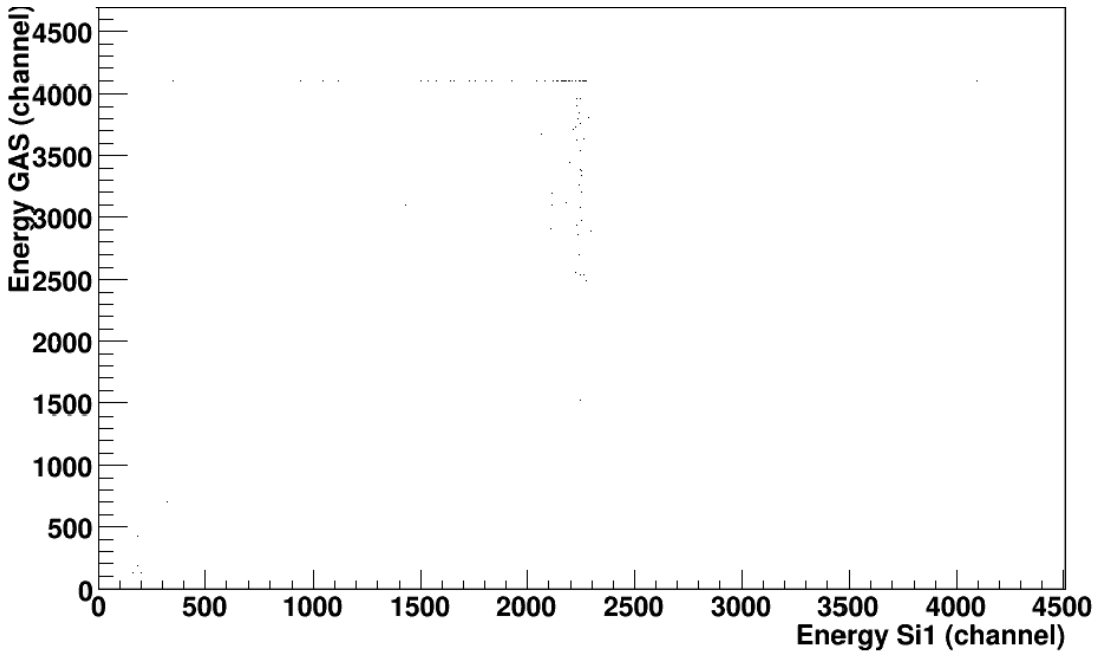

Figure 33: A $\Delta E - E$ plot with the gas detector against Si1 for background measurement, during 86 minutes with closed beam gate. Events with energy equal to channel 0 in the gas detector cannot be seen in this figure.

In Figure 34, the background below 600 keV is fitted to a Landau distribution with a constant equal to 595.915. The most probable value is equal to 327.782 keV and σ = 32.6442 keV. The picture to the right in Figure 34 shows the energy in the low-energy region for the ^{20}Mg decay detected in Si1 with the Landau distribution subtracted. After the subtraction 275 events were detected within $\pm 2\sigma$ around the expected position of the 450 keV protons. If the Landau distribution describes the low-energy background in a correct way, it gives 1.28% $\pm$0.16% proton decay from the 2645 keV level in ^{20}Na. The statistical error in this value is calculated as the square root of the total intensity in the proton peak. Doing the same kind of fit, but only for the energy interval from 350 keV to 600 keV gives 0.98% $\pm$0.16% protons.

With the reduced amount of β-particles from ^{20}Na, as obtained with the gate on time from last beam pulse, 70-200 ms, a subtracted Landau function gives 0.31% $\pm$0.26% protons.

Landau distributions were chosen because they describe the energy fluctuations of not completely stopped charged particles in matter [14]. Though, without knowing the origin of the low-energy background the systematic error in this method can be very large.

No events with matching energy in front side and back side of the DSSSD were found from the background measurement.

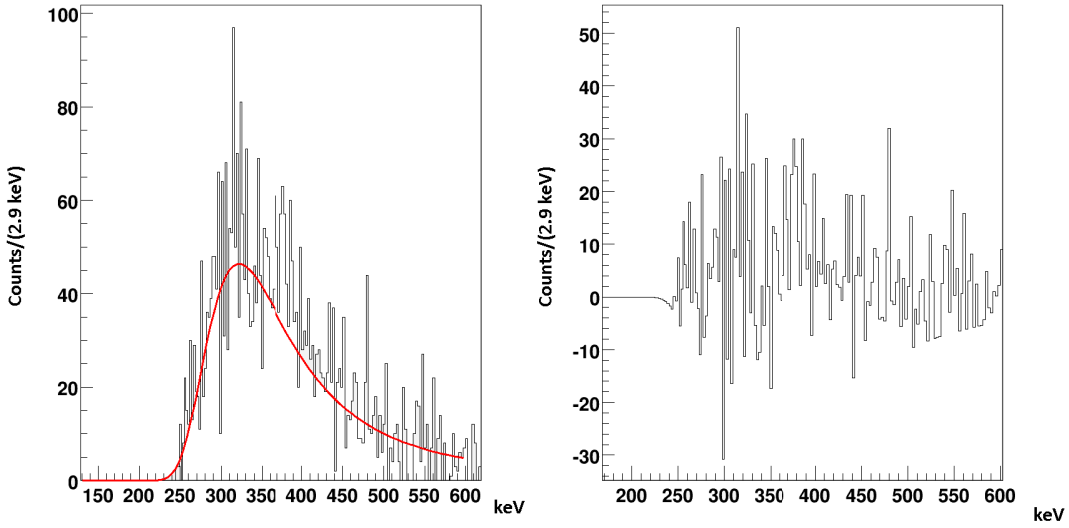

Figure 34: To the left: The low-energy background in the Si1 spectrum with a fitted Landau distribution. To the right: The Si1 spectrum from ^{20}Mg decay with subtracted background.

9 Discussion

The main problem for obtaining a pure low-energy proton spectrum in the first silicon detector seems to be caused by low-energy β-particles. One way to reduce them further would be to have a detector between the DSSSD and the Epad, sufficiently thick to stop high energy protons. Then, a signal in the Epad should guarantee a β-particle on that side (in the case without accidental coincidences or other possible background and noise). Another way of guaranteeing a β^+ on the opposite side of the proton measurement is to use its annihilation and measure the two back-to-back resulting 511 keV photons, in coincidence. The scintillators for annihilation measurement would be placed so that only β^+-annihilation from the wanted side can give coincidences.

This would decrease the amount of statistics, as protons decaying with lower β-energy are stopped in the DSSSD or in the middle detector and are lost. By placing more β-detector setups around the decay, a larger solid angle is covered. That setup can also be used to test the amount of accidental coincidences, collecting the coincident signal of more than one β-detector.

Another possibility would be to have a thinner DSSSD detector. From the ^{21}Na measurement it is seen that in 60 μm silicon, β's up to 500 keV can be detected. With a thinner detector this limit hopefully could be decreased below the energy of the interesting 450 keV proton. To avoid detection of ^{16}O recoils in the DSSSD, a deadlayer thick enough for stopping ^{16}O, but not low-energy protons is desirable.

The 1 μm thick ΔE detectors, mentioned in Section 7, might be a solution if they are combined with β-detectors. Due to the very small area of those ΔE detectors, many of them have to be used in the same experiment and the statistics added together. The reason why this detector has a small active area of 3.5 $\times$ 3.5 mm is to avoid a large capacitance[5]. The number of detectors needed will depend on their distance from the beam.

Another opportunity to reduce β's in the detectors, is to use a magnetic field. This was done by Adelberger et al. in a study of *Positron-neutrino correlation in the* $0^+ -> 0^+$ *decay of* ^{32}Ar

[5]Modeling the detector as a parallel plate capacitor, makes the capacitance proportional to the area divided by the distance between the two plates.

[31]. An estimate of the strength of the magnetic field needed for bending β's but not protons from ^{20}Mg decay is 3 T if the detector is placed between 15 mm and 30 mm from the decay. With 1 T the detector should be placed between 45 mm and 95 mm from the decay. Those calculations are based on the radius of the circular motion of a particle affected by the Lorentz force. Therefore it is also needed that β's with large angle between the detector and the initial velocity can be stopped before they bend towards the detector, through collimators.

As mentioned, the used calibration is not truly valid for energies below 1000 keV. Taking into account more non-linear effects in the lower energy regions may therefore improve the analysis of the 450 keV protons. However, since the non-ionizing part of the energy losses was below about 2 keV for the protons in silicon, the error caused by this is negligible compared to the resolution and the background. As the calibration has been made with α's and protons with energies higher than 1700 keV and compared to known protons with energies larger than 900 keV, the assumption of linear detector response for lower energies could not be verified in this study.

In this analysis, the shape of the energy peaks are assumed to be Gaussian distributions or a sum of several Gaussians. A more precise study of the shape would provide a response function that depends on different energy loss mechanisms for different particles and the geometry of the detector setup.

Further, the exponential energy cuts used for proton separation in the Gas-Si1 plot, shown in Figure 13 are done for raw channel energy. A trustful calibration of the gas detector has not been obtained within this analysis, but might be necessary for improving this cut. Calibration of the gas detector is also needed for a better comparison between the location of real and simulated particles in the $\Delta E - E$ plot.

There might be more than one combination of excited states in ^{20}Na and ^{19}Ne, that result in the same difference in energy. Thereby those sum to the same proton-line. In order to extract log(ft) values from the data, a knowledge of the excitation energy in ^{20}Na is needed. This can be obtain by measuring the decay in coincidence with a γ-detector in a future experiment. The γ-detector measures the energy of the emitted γ when ^{20}Ne decays to the ground state or a lower excited state.

In the setup used for IS507 there is a low probability of detecting γ-photons in the detectors. Thus, events with a photon detected in the Epad in coincidence with a β-particle in the Si1 take part of the low-energy background seen in the proton spectrum of Si1. Photons from the annihilation of β-particles, that are spread via Compton scattering may also be detected in the Epad.

10 Conclusions

No new limits on the population of the resonance level of 2645 keV in ^{20}Na from β-delayed proton emission from ^{20}Mg could be put in this analysis. It was seen that the low-energy region in the Gas-Si1 telescope could not be sufficiently cleaned from background and noise. Furthermore the deadlayer of the DSSSD was too thin to stop recoils of ^{16}O, which prevented identification of low-energy protons.

The gas detector and Si1 could however be used to identify α-particles from ^{21}Mg.

Simulations showed the importance of reducing the contributions of β-particles in the spectra. To improve the detector setup, a 1 μm thick $\Delta E - E$ detector is suggested for future experiments. These shall preferably be used together with β- and γ-detectors.

References

[1] National Nuclear Data Center, *Chart of Nuclides*. http://www.nndc.bnl.gov/chart/ (2012-03-15)

[2] Piechaczek, A et al. (1995) Beta-decay of ^{20}Mg. *Nuclear Physics*, A584 ,509-531

[3] Iliadis, C. (2007) *Nuclear physics of stars*. Germany: WILEY-VCH Verlag GmbH & Co.

[4] Schatz, H. et al. (2001) End point of the rp-process on accreting neutron stars. *Physical review letters*, 86, 16

[5] Krane, K.S. (1988) *Introductory Nuclear physics*. 2nd ed. United States of America: John Wiley & Sons inc

[6] Borge, M.J.G et al (1988) Beta-delayed proton and alpha emission in the decay of ^{17}Ne. *Nuclear Physics*, A490, 287-306

[7] Brown, B.A (2002) The nuclear shell model towards the drip lines. http://www.nscl.msu.edu/~brown/pub/papers/R277.pdf (2012-03-19)

[8] Brown, B.A. et al. (1993) Nature of the ^{20}Na 2646 keV level and the stellar reaction rate for ^{19}Ne(p,γ)^{20}Na. *Physical Review*, C48, 1456

[9] Seweryniak, D. (2004) Complete structure determination of the astrophysical important nucleus ^{20}Na below the proton threshold. *Physics Letters*, B590, 170-175

[10] Lam et al. *Empirical Isospin Symmetry Breaking Hamiltonians for sd-Shell*. http://indico.in2p3.fr/getFile.py/acess?resId=6&materialId=paper&confId=4091 (2012-03-15)

[11] Harakeh, M. N. and van der Woude, A. (2001) *Giant Resonances Fundamental High-Frequency Modes of Nuclear Excitation*. Oxford: Clarendon press

[12] Wójcik, M. and Drożdż, S. (1998) Configuration mixing effects in isoscalar giant dipole resonace. *Acta physica polonica B*, 29, No 9, 2239-2244

[13] Ziegler, J. F *SRIM The Stopping and Range of Ions in Matter*. http://www.srim.org/SRIM/SRIMINTRO.htm (2012-03-15)

[14] Leo, W.R. (1987) *Techniques for nuclear and particle physics experiments*. Germany: Springer-Verlag Berlin Heidelberg

[15] Holifield radioactive ion beam facility, *Double sided silicon strip detectors (DSSSD)*. http://www.phy.ornl.gov/hribf/research/equipment/rms/dsssd.html (2012-03-15)

[16] Logbook for experiment IS507 CERN-ISOLDE (2011)

[17] Mishin, V.I. et al. (1993) Chemically selective laser ion.source for the CERN-ISOLDE on-line mass separator facility. *Nuclear instruments and methods in physics Research*, B73, 550-560

[18] Borge, M.J.G, (2010) *Study of the β-decay of ^{20}Mg* Proposal to the INTC

[19] Johansson, H. (2010) *Hunting tools beyond the driplines*. Göteborg: Chalmers Reproservice

[20] The ROOT team *About ROOT*. http://root.cern.ch/drupal/content/about (2012-03-23)

[21] Honkanen, A. et al. (1996) Fine structure in the beta-delayed proton decay of ^{33}Ar. *Nuclear physics*, A611, 47-55

[22] Sextro, R.G, Gough, R.A and Cerny, J. (1973) β^+-delayed proton decay of ^{21}Mg. *Physical review*, C8, 258-268

[23] Kirsebom, O.S. et al. (2011) Precise and accurate determination of the 8B decay spectrum. *Physical Review*, C83, 065802

[24] Tengborn, E. (2009) *Transfer reactions in inverse kinematics at REX-ISOLDE*. Göteborg: Chalmers Reproservice

[25] Tengblad, O et al. (2004) Novel thin window design for a large-area silicon strip detector. *Nuclear instruments and methods in physics research*, A525, 458-464

[26] Nordling, C. & Österman, J. (1987) *Physics Handbook*. 4th ed. Sweden: Studentlitteratur

[27] Wilson, R.G, (1967) Surface ionization ion sources. *IEEE transactions on nuclear science*

[28] Giles, T.J. et al. (2003) The high resolution spectrometer at ISOLDE *Nuclear instruments and methods in physics research*, B204, 497-501

[29] Application software group computing and network division CERN *GEANT Detector description and simulation tool*. `http://wwwasdoc.web.cern.ch/wwwasdoc/pdfdir/geant.pdf` (2012-04-07)

[30] R310 Monolitithic silicon detector telescope (1996) *SGS-Thomson micrelectronics*, Italy.

[31] Adelberger, E.G. et. all. (1999) Positron-neutrino correlation in the $0^+ - > 0^+$ decay of ^{32}Ar. *Physical Review*, 83, 7, 1299-1302.

A Proton peak positions

Si1

^{21}Mg	E [keV]	σ [keV]	♯ events within $\pm 2\sigma$	Rel. intensity	Rel. intensity Previous [2]
	898	64.02	540	0.209	
	1045	36.37	201	0.078	
	1258	17.61	531	0.206	
	1496	24.55	156	0.060	
	1773	19.02	1177	0.456	
	1939	24.78	2581	1	
	2472	71.00	472	0.183	
	3291	19.63	181	0.070	
	3855	12.12	114	0.044	
	4675	21.31	398	0.154	
^{20}Mg					
	746	25.9	965	1	1
	1573	30.1	627	0.650	0.417
	1796	36.6	78	0.081	0.096
	2455	56.7	196	0.203	0.261
	2968	27.1	53	0.055	-
	3861	43.0	130	0.135	0.140
	4102	21.5	116	0.120	0.156

DSSSD

^{21}Mg	E [keV]
	878
	1056
	1252
	1489
	1773
	1940

B DSSSD calibration parameters

Strip	Offset [keV]	Gain [keV/channel]	Mean distance through Si deadlayer [μm]
Front 1	-244.804	2.0021	0.116095
Front 2	-197.735	1.9743	0.112871
Front 3	-190.445	1.8319	0.110281
Front 4	-253.459	1.9320	0.108373
Front 5	-258.306	1.8901	0.107185
Front 6	-187.614	1.9040	0.106745
Front 7	-209.817	1.8399	0.107062
Front 8	-197.907	1.8643	0.108128
Front 9	-220.728	1.8804	0.109921
Front 10	-214.516	1.8699	0.112403
Front 11	-213.486	1.8497	0.115526
Front 12	-240.058	1.8717	0.119237
Front 13	-268.033	1.8995	0.123481
Front 14	-235.093	1.8223	0.128202
Front 15	-259.803	1.9012	0.133347
Front 16	-203.816	1.9759	0.138870
Back 1	-202.273	1.8334	1.049240
Back 2	-232.035	1.8074	1.009860
Back 3	-289.225	1.8382	0.974100
Back 4(dead strip)	-	-	-
Back 5	-265.362	1.8698	0.915200
Back 6	-198.963	1.8166	0.892970
Back 7	-243.141	1.7970	0.876110
Back 8	-264.600	1.8476	0.864970
Back 9	-288.022	1.8041	0.859810
Back 10	-230.549	1.8292	0.860724
Back 11	-237.663	1.8111	0.867710
Back 12	-208.049	1.8758	0.880601
Back 13	-259.912	1.8812	0.899119
Back 14	-259.242	1.82415	0.922892
Back 15	-233.739	1.76867	0.951493
Back 16	-299.242	1.8429	0.984467